Report to

NATIONAL SCIENCE FOUNDATION
Washington, D.C.
Grant No. ENV77-15333

EARTHQUAKE RESISTANT STRUCTURAL WALLS
ANALYSIS OF COUPLED WALL SPECIMENS

by

T. Takayanagi
A. Scanlon
W. G. Corley

Submitted by

CONSTRUCTION TECHNOLOGY LABORATORIES
A Division of the Portland Cement Association
5420 Old Orchard Road
Skokie, Illinois 60077

July, 1981

50272-101

REPORT DOCUMENTATION PAGE	1. REPORT NO. NSF/CEE-81067	2.	3. PB82-149048

4. Title and Subtitle	5. Report Date
Earthquake Resistant Structural Walls Analysis of Coupled Wall Specimens, Final Report	July 1981
	6. 4007128

7. Author(s)	8. Performing Organization Rept. No.
W.G. Corley, T. Takayanagi, A. Scanlon	

9. Performing Organization Name and Address	10. Project/Task/Work Unit No.
Portland Cement Association Construction Technology Laboratories 5420 Old Orchard Road Skokie, IL 60077	
	11. Contract(C) or Grant(G) No. (C) (G) ENV7715333

12. Sponsoring Organization Name and Address	13. Type of Report & Period Covered
Directorate for Engineering (ENG) National Science Foundation 1800 G Street, N.W. Washington, DC 20550	Final
	14.

15. Supplementary Notes

16. Abstract (Limit: 200 words)

A structural model that can predict the response history and failure mechanisms of coupled wall systems under static loads is described. The analytical results are compared with test results for coupled wall specimens tested at the Construction Technology Laboratories. On the basis of this comparison, effects of assumed analytical conditions on overall behavior are discussed. The analytical results are in agreement with the experimental results with respect to overall behavior of the wall systems considered. It was demonstrated that analytical models can simulate important aspects of behavior of constituent members of coupled wall systems. The appendices include discussions on (1) development of member analytical models; (2) the assemblage of the structural stiffness matrix and calculation of failure mechanism formation; and (3) a static analysis of isolated structural walls.
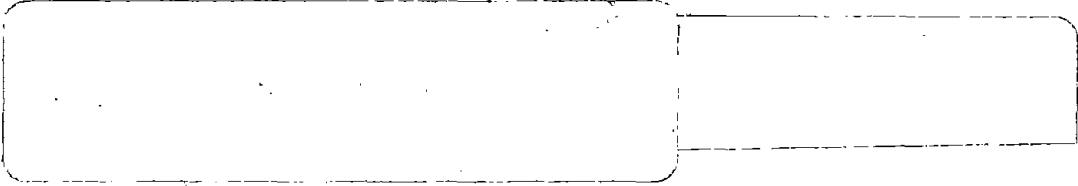
17. Document Analysis   a. Descriptors

Earthquake resistant structures   Static loads
Walls   Concrete structures
Static structural analysis   Deformation methods
Buildings

b. Identifiers/Open-Ended Terms   Shear walls
Coupled walls
W.G. Corley, /PI

c. COSATI Field/Group

18. Availability Statement	19. Security Class (This Report)	21. No. of Pages
NTIS	20. Security Class (This Page)	22. Price

(See ANSI-Z39.18)	See Instructions on Reverse	OPTIONAL FORM 272 (4-77) (Formerly NTIS-35) Department of Commerce

TABLE OF CONTENTS

TABLE OF CONTENTS (CONTD.)

EARTHQUAKE RESISTANT STRUCTURAL WALLS
ANALYSIS OF COUPLED WALL SPECIMENS

by

T. Takayanagi,[1] A. Scanlon,[2] and W. G. Corley[3]

INTRODUCTION

Reinforced concrete structural walls provide a means of stiffening multistory buildings against earthquake-induced lateral loads. Of particular interest are coupled wall systems consisting of two walls connected by beams. Connecting beams can effectively dissipate energy by formation of inelastic hinges at beam ends.

In general, coupled wall systems can be characterized by two primary structural actions. These are flexural resistance of individual walls and coupling resistance due to axial force acting in the walls. Axial force in the walls is the accumulation of forces transmitted through shear forces in connecting beams. The degree of coupling is directly dependent on capacity of the connecting beams.

To investigate performance of coupled wall systems under lateral load, an experimental program was conducted at the Construction Technology Laboratories. An analytical investigation was also undertaken to simulate behavior of the test specimens using computer modelling techniques. This report describes the analytical phase of the investigation.

---
(1)Former Senior Structural Engineer, and (2)Manager, Analytical Design Section, (3)Divisional Director, Engineering Development Division, Portland Cement Association, Skokie, Illinois.

Analytical models for constituent members of a coupled wall system and a procedure to assemble these member models into an overall structural model are presented. The basic member models used in this report are modified versions of flexural line elements. They include specific features of the walls and connecting beams in addition to the conventional flexural yielding feature. These specific features are: 1) interaction between moment and axial force in the walls, 2) coupling between shear and moment in the walls and connecting beams, and 3) rotation due to strain in beam tensile reinforcement embedded in the wall.

For a member subjected to moments and axial forces that change in the process of loading, neither moment-curvature nor axial stress versus axial strain relationships can be uniquely determined in advance. The reason for this is that the inelastic axial action and flexural action are coupled. Structural response depends on the ratio of axial load to moment acting on a member. Details of this behavior are discussed in Appendix A.

Experimental results (2,7) have indicated that shear yielding and flexural yielding are also coupled in the form of an almost-simultaneous occurrence of shear yielding and flexural yielding. This coupling behavior is explained in detail in Appendices A and C.

Strain in beam tensile reinforcement embedded in the wall can be significant in reducing the overall stiffness of coupled wall systems, especially for systems with strong beams. Treatment of this effect is described in Appendix A.

Hysteretic properties of constituent elements are established by utilizing, and modifying where necessary, available hysteresis rules.

Response of coupled wall systems to lateral loads is calculated using the developed analytical procedure. In the analysis, a stiffness updating process is carried out on each constituent member in a step-by-step manner.

Finally, calculated results are compared to experimental results. The influence of various parameters that control the response of coupled wall systems is discussed based on the comparison between the experimental and analytical results.

ANALYTICAL MODELS

General

Realistic modelling of member behavior is essential for analytical models to accurately predict the overall behavior of structural systems under loading. For reinforced concrete structures under reversed loading, the member properties include primary curve shapes and hysteretic characteristics defining force-deformation relationships at member ends.

There are three possible approaches to evaluate reinforced concrete member properties. The first approach relies on purely analytical treatment based on stress-strain relationships of concrete and reinforcement and the geometrical configuration of the member. This approach requires data pertaining to tri-axial stress history, strain discontinuities associated with cracking, bond slip, and so forth.

The second approach is based on the cross-sectional proper-ties of members. Instantaneous stiffness of a member can be evaluated by integrating the rigidity distribution along the member axis. However, it is difficult to consider effects such as crack opening, bond slip, and inclined cracks in this approach.

The third approach is to utilize force-deformation relation-ships obtained in tests on beam specimens under simple loading conditions.

In this investigation, all three approaches have been used in different aspects of the modelling procedure. For example,

analytical models based on stress-strain relationships of materials have been used to model flexural properties, and interaction between axial behavior and flexural behavior. On the other hand, properties associated with shear action, such as primary curve of shear-versus-shear-distortion relationship and coupling between shear yielding and flexural yielding are based on experimental results. Hysteretic characteristics of various types of force-deformation relationship are also based on experimental results.

Structural Idealization

The lateral resistance of a coupled wall system consists of two primary structural actions: flexural resistance of individual walls and the coupling moment due to axial forces acting in the walls. Axial force in a wall is the accumulation of shear forces transmitted through the connecting beams.

Walls and connecting beams are replaced by line members at their centroidal axes. The wall members have flexural, axial and shear rigidities as their member stiffness components. The connecting beam members have flexural and shear rigidities. Three displacement components are considered at each wall-beam joint: horizontal displacement, vertical displacement and rotation. Walls are assumed to be fully fixed at the base. The structural model of the coupled wall systems analyzed in this investigation is shown in Fig. 1.

The combined two cantilever beam model[10] has been adopted for the connecting beams. The beam consists of two cantilever beams whose free ends are placed at the inflection
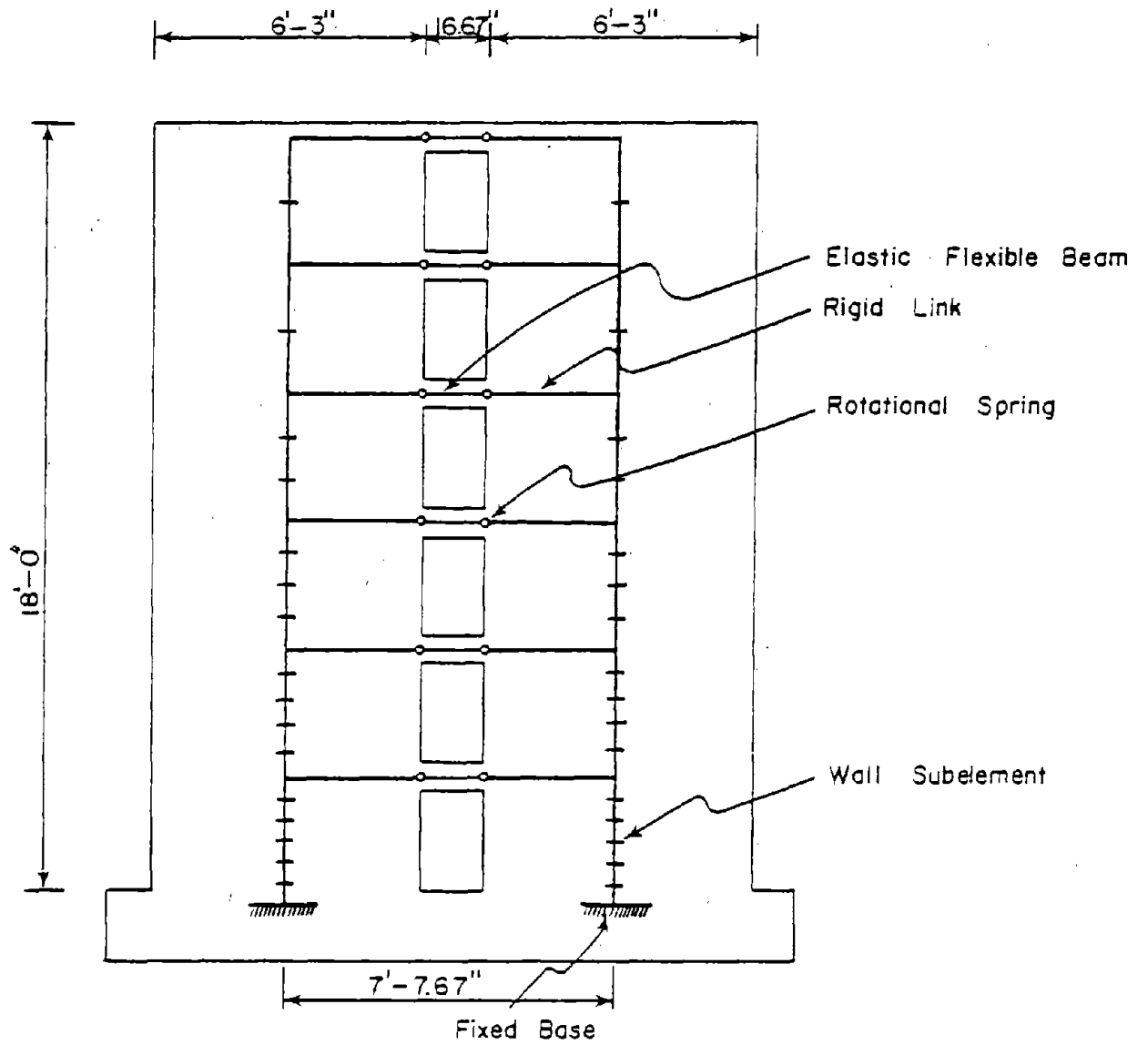
Fig. 1 Structural Model of Coupled Wall Systems

point. The model is quite suitable for the connecting beams of a coupled wall system, since the inflection point is practically fixed at the midspan of the beam during the loading process. The beams are connected to each wall through a rigid link and a rotational spring as shown in Fig 1.

The rotational spring models beam end rotation due to the steel bar elongation and concrete compression in the joint core area as well as the inelastic flexural and shear actions over the beam length. Such inelastic actions are expected to be localized near the beam ends because of the antisymmetric distribution of moment over the beam length. The beam itself is considered to be a flexural member with uniform elastic rigidity along its length.

Wall members are subjected to a more general distribution of moments than the connecting beams. Also, the change of axial force during the loading process can cause a change of moment capacity in the wall members. Therefore, inelastic flexural behavior in the wall can be expected to expand along the length of the member rather than be localized at the ends as for the connecting beams.

To allow the inelastic action to expand over a partial length of wall member, the member is further divided into several subelements as shown in Fig. 1. The degree of subdivision decreases with story height since the major inelastic action is expected at the base. The finer arrangement of subelements allows closer idealization of localized inelastic action at that part.

Details of the procedure used to develop the analytical models for constituent members are discussed in Appendix A.

Calculation Procedure

A method of analysis for reinforced concrete coupled wall systems subjected to large reversing loads or monotonically increasing loads is described here. The method of analysis was developed to investigate inelastic behavior of a coupled wall system when the system is loaded into a highly inelastic range.[8]

Instantaneous stiffness components of each member are evaluated on the basis of the force-deformation relationships of the beam rotational springs and wall subelements. The force-deformation relationships follow a specified set of hysteresis rules.

The instantaneous structural stiffness matrix is developed by assembling the instantaneous member stiffnesses. Inelastic behavior of the structure under static loads is evaluated by applying loads incrementally. The instantaneous structural stiffness is assumed to be constant within a small load step. Geometric nonlinearity is ignored in the analysis. Therefore, the structural analysis can be based on the initial configuration.

Details of the assemblage process of the structual stiffness matrix and the calculation process tracing the formation of failure mechanisms are explained in Appendix B.

Computer Programs

Two computer programs, SIVA1 and SIVA2, were used for this investigation. Program SIVA1 performs static analysis of coupled wall systems. Program SIVA2 is specialized for static analysis of isolated structural walls. These programs were originally developed at the University of Illinois at Champaign-Urbana[8], and modified at the Construction Technology Laboratories by T. Takayanagi.

Analysis procedures are described in Appendices A and B. The programs have the capability to perform inelastic static analysis of structural walls under monotonic or reversed loading in a step-by-step manner. The programs are limited to analysis of structural walls with up to 10 stories. A wall member can be divided into subelements in any arrangement up to 7 elements.

Takeda's hysteresis rules[11] with the options relating to strength loss, "pinching" effect, coupling between shear and flexural components, and interaction between axial and flexural components have been adopted in the programs. Calculated story force-displacement curves of the structure can be plotted at the end of the calculations.

STATIC ANALYSIS

Preliminary Remarks

The analytical procedure outlined in the previous chapter was applied to the coupled wall systems tested at the Construction Technology Laboratories. Two systems denoted by CS-1 and RCS-1 were selected for analysis. RCS-1 is the repaired system of CS-1 in which the coupling beams were replaced with stronger beams after these original beams were extensively damaged in the test of CS-1. Test details are described in Ref. 12.

Static analyses were performed to evaluate the influence of various parameters on the behavior of coupled wall systems under large statically applied loads. Overall validity of the analytical models was confirmed by comparing analytical results with experimental results.

The analytical procedure was also applied to simulations of isolated wall tests conducted at the Construction Technology Laboratories.[7] These analyses were made to verify the capability of the wall member models to simulate inelastic behavior of isolated walls. Emphasis was placed on the effect of coupling between flexural yielding and shear yielding on the overall behavior of isolated walls. Results of the analysis as well as the comparison between analytical and test results are described in detail in Appendix C.

Idealization of Coupled Wall Specimens

Dimensions of the coupled wall systems are shown in Fig. 1. Two identical rectangular walls are connected by six beams to

represent a six-story coupled wall. Each wall has a height of 18 ft (5.5 m), a horizontal length of 6 ft 3 in. (1.9 m), and a thickness of 4 in. (106 mm). Beams are spaced uniformly along the height at 3 ft (0.9 m) centers. They have a span of 16-2/3 in. (423 mm) and a width of 4 in. (106 mm).

For system CS-1, beams have a depth of 6-2/3 in. (169 mm) and a width of 4 in. (106 mm). For repaired system RCS-1, beams have a depth of 8 in. (203 mm) and a width of 10 in. (254 mm). Floor slabs are simulated by 2.5 in. (64 mm) by 1 ft (0.3 m) wide stubs running the full length of the specimen on both sides. Details of the specimens, such as material properties, reinforcement arrangement, and test setup are described in Ref. (12).

For the computer analysis, walls and beams of the specimens are idealized as line members at their centroidal axes as shown in Fig. 1. Connecting beams are modelled by an inelastic rotational spring and a rigid segment at each end. An elastic element is placed between the springs. Wall elements are divided into segments for more accurate modelling of inelastic behavior within a story height. Details of the models are discussed in Appendix A.

The walls are assumed to be fixed at the base. Loads are applied laterally in small increments at the top of the coupled wall system. The load increment used in the analysis is 1/200 of the maximum static load applied.

Primary Parameters

Effects of the following parameters on behavior of coupled wall systems were investigated: (1) inelastic shear behavior with coupling between flexural yielding and shear yielding in the walls, (2) interaction between flexural behavior and axial behavior in the walls, (3) inelastic shear behavior in the beams, (4) rotation due to strain in embedded reinforcement at the beams ends, (5) pinching and strength loss in the beams.

Primary curves for the force-deformation relationships of the beam rotational springs and wall subelements were determined by the procedure outlined in Appendix A. Parameters defining the primary curves used in the analysis are summarized in Table 1. Uncracked wall and beam properties are uniform over the height of the structures. The wall properties of Specimen RCS-1 were determined based on test results for CS-1.

Analysis of Elements

Analysis of each constituent element under monotonically increasing load was conducted prior to analysis of coupled wall systems to determine the inelastic deformation characteristics of the elements. Effects of parameters such as inelastic shear deformation and rotation due to tensile strain of embedded reinforcement on the overall force-displacement relationships of the elements are investigated by comparison with available element test results.

Results of the element analyses are used for the subsequent analysis of coupled wall systems.

TABLE 1 PRIMARY CURVE PROPERTIES OF
CONSTITUENT ELEMENTS

		CS-1	RCS-1
Wall Subelement			
Elastic Axial Rigidity	(kip)	1,113,000	1,113,000
Axial Rigidity of a Fully Cracked Section[1]	(kip)	139,000	139,000
Shear Versus Shear Distortion Curve			
First Slope	(kip)	300,000	23,000 [4]
Second Slope	(kip)	23,000	–
Third Slope	(kip)	400	400
Cracking Shear	(kip)	20	–
Shear Strength	(kip)	90	–
Moment Versus Curvature Curve			
First Slope	$(kip-in^2)$	708,000,000	220,000,000 [5]
Second Slope	$(kip-in^2)$	186,000,000	–
Third Slope	$(kip-in^2)$	2,600,000	2,600,000
Cracking Moment	(kip-in)	2,300	–
Yielding Moment	(kip-in)	12,000	12,000
Beam Rotational Spring			
First Slope[2]	(kip-in)	1,300,000 235,000 [3]	6,120,000 2,450,000 [6] 1,710,000 [7]
Second Slope	(kip-in)	126,000 3,900 [3]	1,390,000 556,000 [6] 335,000 [7]
Third Slope	(kip-in)	1,000 500 [3]	12,000 4,800 [6] 4,600 [7]
Cracking Moment	(kip-in)	16	55
Yielding Moment	(kip-in)	47	350

(1) Only the reinforcement contribution is considered in the calculation of axial rigidity.

(2) Actual meaning of the value is 6EI/L if effects of strain in embedded reinforcement and inelastic shear deformation are not considered.

(3) Effects of strain in embedded reinforcement and inelastic shear deformation are considered.

(4) No uncracked stages are considered since the walls have been cracked in
(5) the test of CS-1. Therefore, the primary curves are bilinearized rather than trilinearized.

(5) Reduced flexural rigidity is assumed based on the results of CS-1 test.

(6) Effect of inelastic shear deformation is considered.

(7) Effects of strain in embedded reinforcement and inelastic shear deformation are considered.

-13-

Beam Element Analysis. Effects of inelastic shear deforma-
tion and rotation due to strain in embedded reinforcement, on
the load-deflection relationship of a beam member are investi-
gated using the analytical model for beams described in Appendix
A. Calculated results are compared with results of coupling
beam tests[13].

Beam Specimen C2 in Ref. 13 was selected for the comparison.
Dimensions of Specimen C2 are the same as those of coupling
beams of CS-1. However, the amount of flexural reinforcement of
C2 is twice as much as that of CS-1. No companion specimen was
made for the coupling beams of CS-1.

Although Specimen C2 does not represent, in the strict
sense, the coupling beams of CS-1, it was decided to conduct the
analysis of C2 as a part of the constituent element analysis.
Analysis of Specimen C2 provided information on the effects of
inelastic shear deformation and rotation due to strain in
embedded reinforcement. The analysis also provided confirmation
of the validity of the beam model used for the analysis of cou-
pled wall systems.

The measured load-deflection envelope of Specimen C2 is com-
pared in Fig. 2 with calculated values. The calculated curves
represent three separate analyses. In the first analysis, only
flexural deformations are considered as contributing to the
deflection. In the second analysis, flexural and shear deforma-
tions are considered. In the third analysis, rotations due to
strain in embedded reinforcement are included in addition to
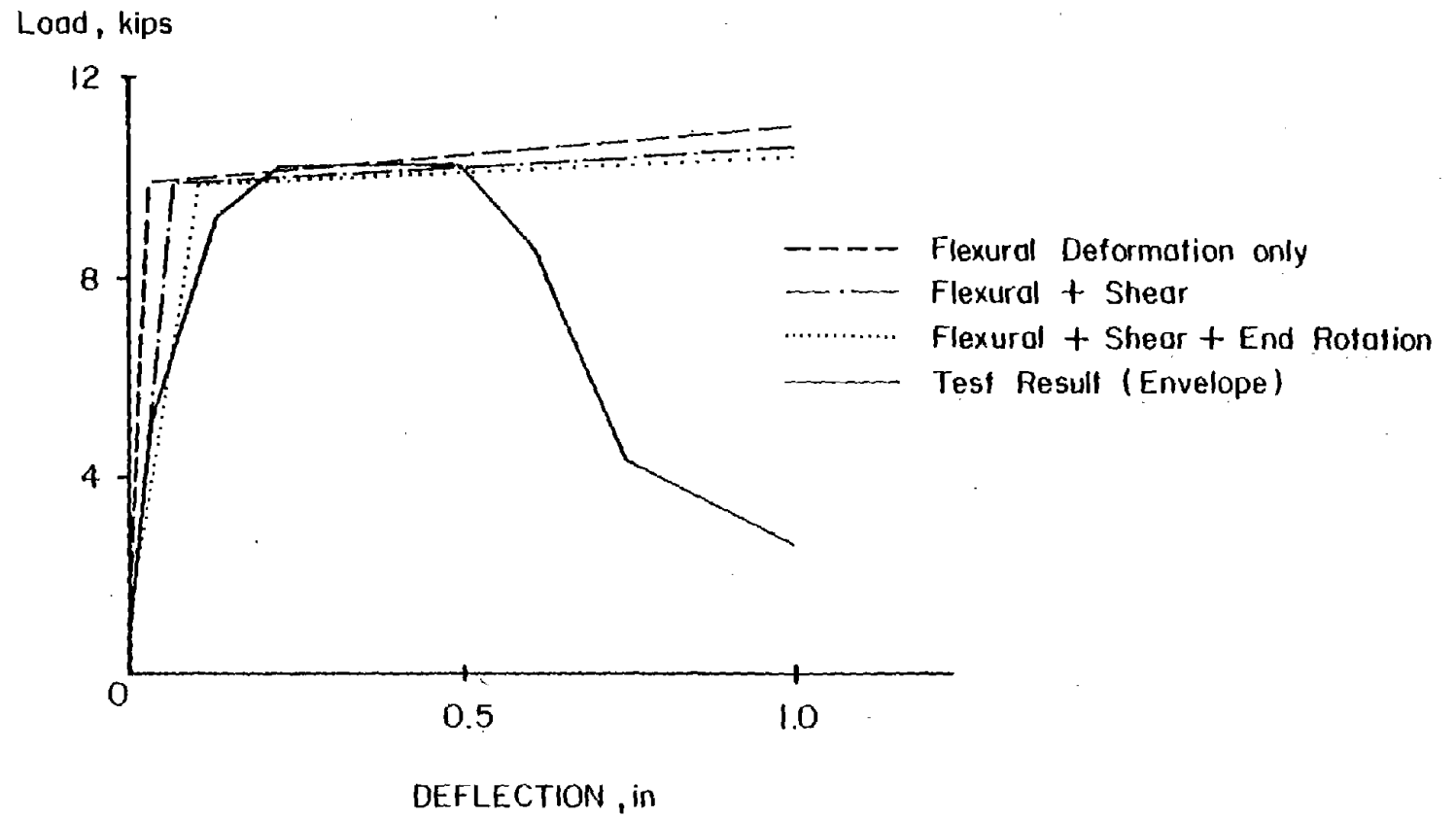flexure and shear deformations.

-14-

Load, kips

Fig. 2 Load-Versus-Deflection Relationship of
Beam Specimen C2 of Ref. 13

It can be seen from Fig. 2, that the inelastic shear deformation and rotation due to strain in embedded reinforcement play a significant role in reducing the rotational stiffness of the coupling beams. The case where the inelastic shear deformation and rotation due to strain in embedded reinforcement are included provides the best agreement with the measured curve.

Wall Element Analysis. A comparison was made between results of isolated wall tests[14] and results obtained using the analytical model for wall members.

The isolated wall specimen selected for analysis represents the individual wall of a coupled wall system and has the same details used for the coupled walls. The specimen was subjected to monotonically increasing loads applied at the top. The wall member properties of CS-1 listed in Table 1 were used for the analysis of the isolated wall specimen.

Figure 3 shows a comparison between two calculated load-deflection curves and the measured curve. The broken line represents the case where no inelastic shear deformation was considered in the analysis. The line-dot line shows the case where inelastic shear deformation was taken into account. It can be seen that inelastic shear deformation had a significant effect before flexural yielding occurred.

Analysis of Coupled Wall Systems

Inelastic response of the coupled wall Systems CS-1 and RCS-1 under static loads was calculated by the analytical procedure described in this report. Results of the calculations
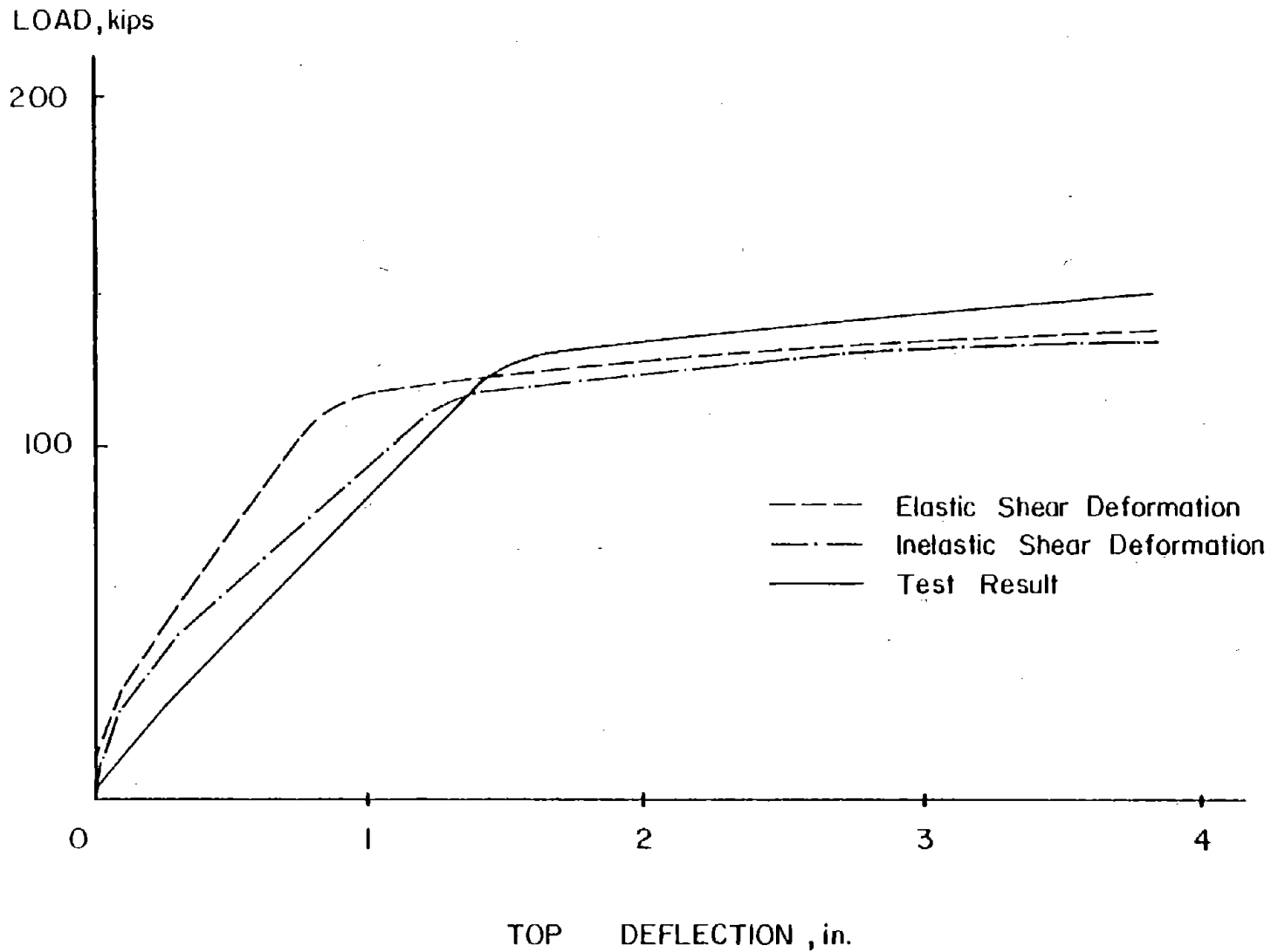
-16-

Fig. 3   Load-Versus-Top-Deflection Relationship of
          Isolated Wall

are compared with experimental results. Unless otherwise stated, loads were applied in monotonically increasing fashion.

Parameters of primary interest in this analysis are inelastic shear deformations in the walls and beams, interaction between axial and flexural actions in the walls, and beam end rotation due to strain in embedded reinforcement. Loads were applied at the top of the wall system in small increments.

Load-Versus-Top-Floor-Displacement Relationships. Load-versus-top-floor-displacement relationships were calculated to identify the effects of several parameters on overall behavior of the systems. Calculated curves for CS-1 and RCS-1 are compared with the corresponding experimental results in Figs. 4 and 5, respectively.

Test results shown in Figs. 4 and 5 are envelopes of repeated loading history curves. The curves represent average results for the two walls tested. For CS-1, effects of end rotation due to strain in embedded reinforcement and inelastic shear deformation are combined since the contribution of the beams to overall behavior of the system is relatively small. On the other hand, for RCS-1, effects of end rotation and inelastic shear are shown separately in Fig. 5.

In Figs. 4 and 5, the entry "Yes" means that the effect described in the column heading was included in the analysis. "No" means that the effect was not included. "Interaction" means that the effect of axial force changes on the inelastic flexural rigidity and the effect of curvature changes on the

LOAD, kips

150

100

50

	BEAM	WALL	
	End Rotation & Inelastic Shear	Interaction	Inelastic Shear
—·—	Yes	Yes	No
············	No	Yes	Yes
———	Yes	Yes	Yes
—··—	Yes	No	Yes
———	Test Result		

0   0.5   1.0   1.5   2.0   2.5

TOP DEFLECTION , in.

Fig. 4   Load-Versus-Top-Deflection Relationship of CS-1

LOAD, kips

200

100

	BEAM		WALL
	End Rotation	Inelastic Shear	Interaction
—··—	No	Yes	No
··········	No	No	Yes
—·—·	No	Yes	Yes
———	Yes	Yes	Yes
———	Test Result		

0   1.0   2.0   3.0   4.0
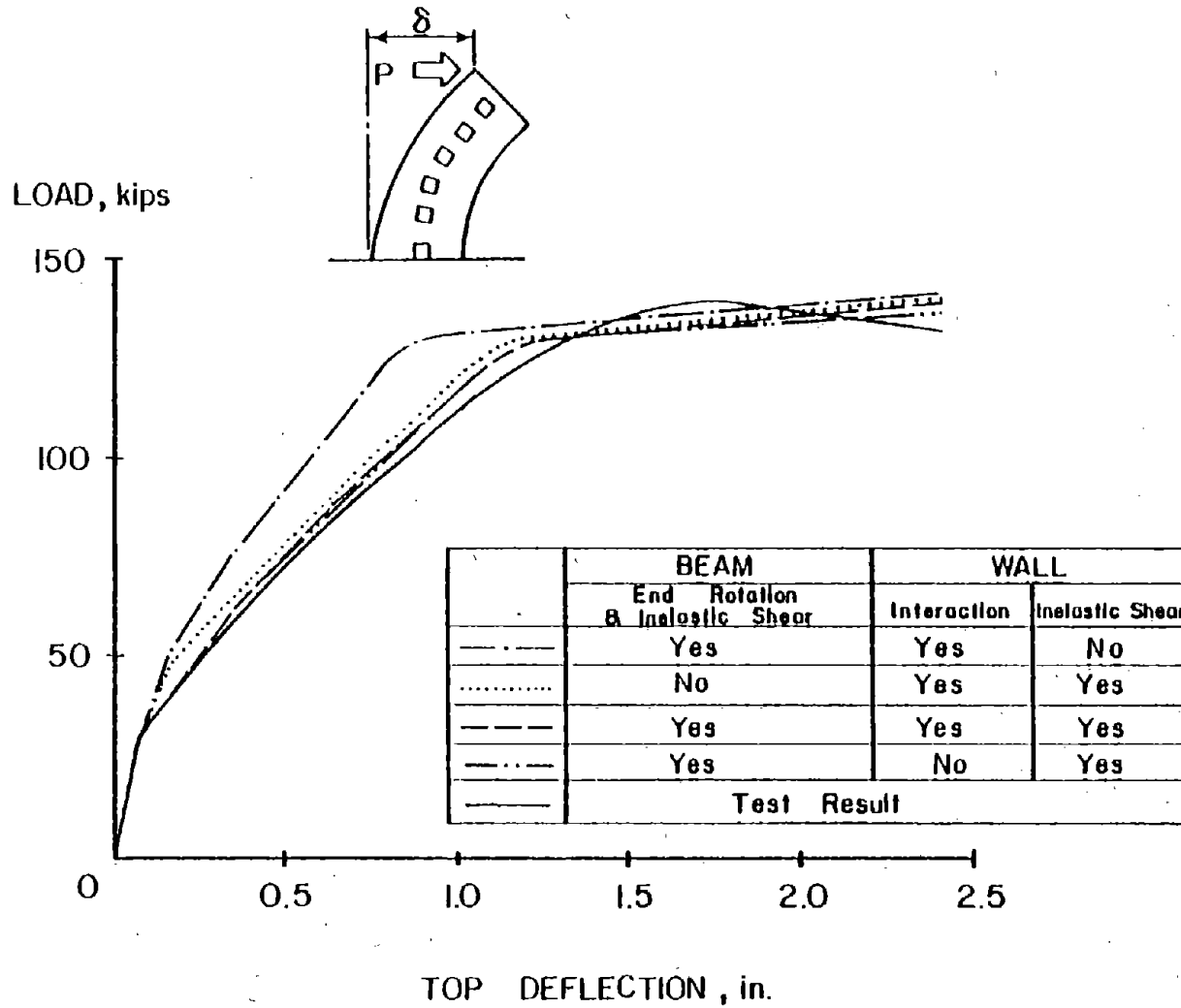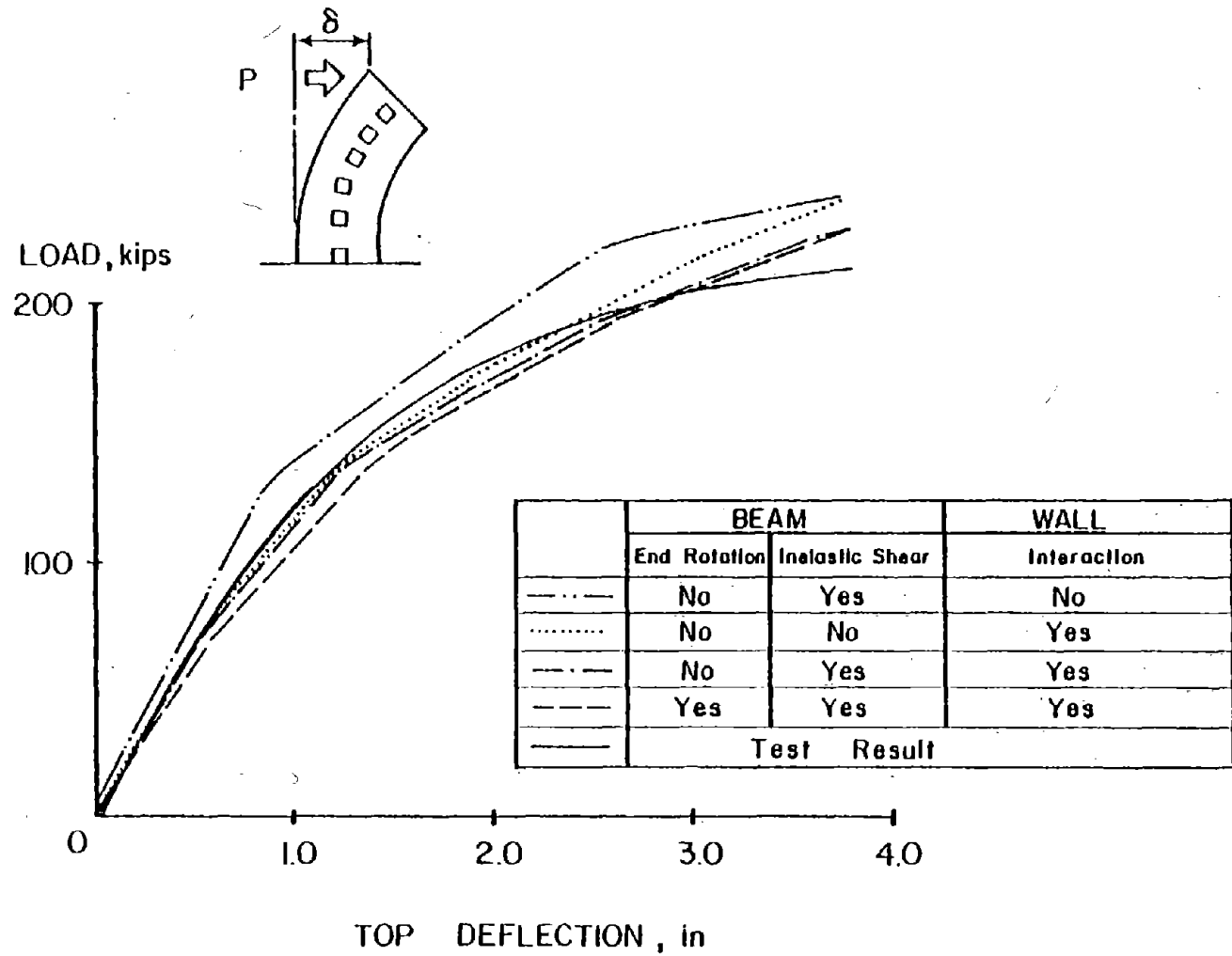
TOP   DEFLECTION , in

Fig. 5   Load-Versus-Top-Deflection Relationship of RCS-1

inelastic axial rigidity in the walls are included. For the case where the interaction effect is not included, elastic axial rigidity is assumed throughout the analysis and no flexural rigidity change due to axial force change is considered.

When the effect of a particular parameter is examined in the analysis, only that parameter is changed while all other parameters are held constant.

As shown in Fig. 4, the effect of inelastic shear deformation in the walls on the overall behavior of CS-1 is so significant that without this effect a comparison between the analytical results and the test results is poor. On the other hand, effects of other parameters pertinent to coupling beams appear nominal compared to the inelastic shear effect in the walls. This can be explained by the fact that weak connecting beams used for CS-1 produce a system that behaves like two isolated walls in parallel.

However, in the analysis of RCS-1, it is apparent that coupling between the two walls plays a significant role in determining the behavior of the system because of strong connecting beams used for the repaired system.

As shown in Fig. 5, if the interaction effect is not included in the analysis, the comparison between test and analytical results is poor. On the other hand, effects of end rotation due to strain in embedded reinforcement and inelastic shear deformation in the connecting beams are not as significant as the interaction effect.

Since no strength loss in the post-yield range is considered in the analysis, the calculated results of the beam strength overestimate the observed results at large deflections.

In the following, inelastic behavior of the coupled wall systems is discussed on the basis of calculated results for the case where all the major parameters identified so far are included in the analysis.

Base-Axial-Force-Versus-Top-Vertical-Displacement Relationship of Walls. In the process of loading, axial stiffness of wall members changes substantially reflecting the cracking or crushing of the concrete and yielding of the reinforcement. Figures 6 and 7 show the relationships between axial force at the base and vertical displacement at the top of walls for CS-1 and RCS-1, respectively.

The displacement at the top of a wall is the accumulation of vertical deformation over the wall height. Also, axial force at the base is the accumulation of coupling force transmitted through the connecting beams. Therefore, the curves show the general trend of inelastic axial behavior of wall members.

Cases where the axial stiffness is assumed to be elastic and constant during loading are also shown in Figs. 6 and 7 to serve as a basis for evaluation of the effect of inelastic axial stiffness in the walls. Since no interaction effects are included, the curves based on elastic axial stiffness are symmetrical about the origin.
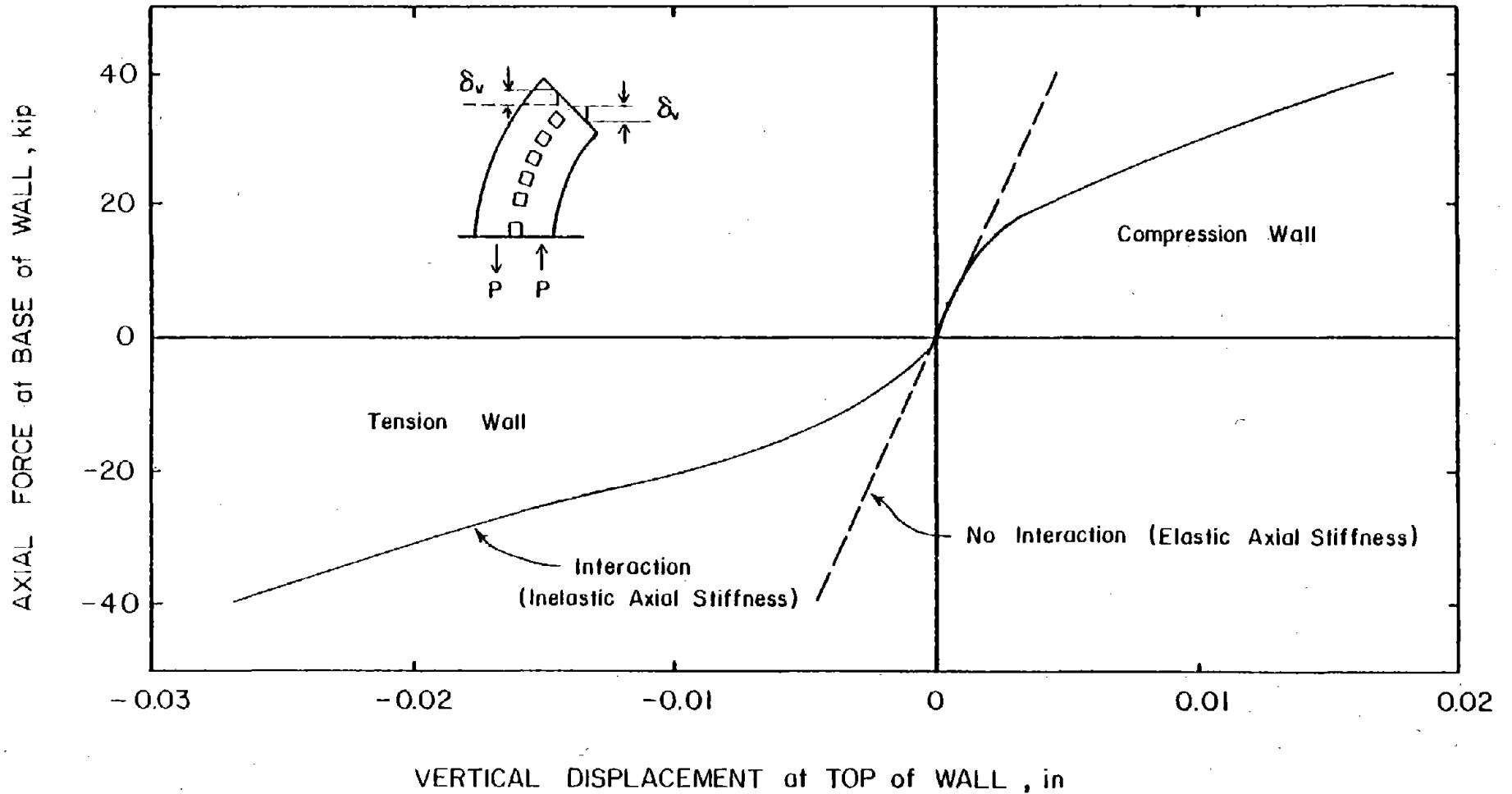
Fig. 6   Calculated Axial-Force-Versus-Vertical-Displacement
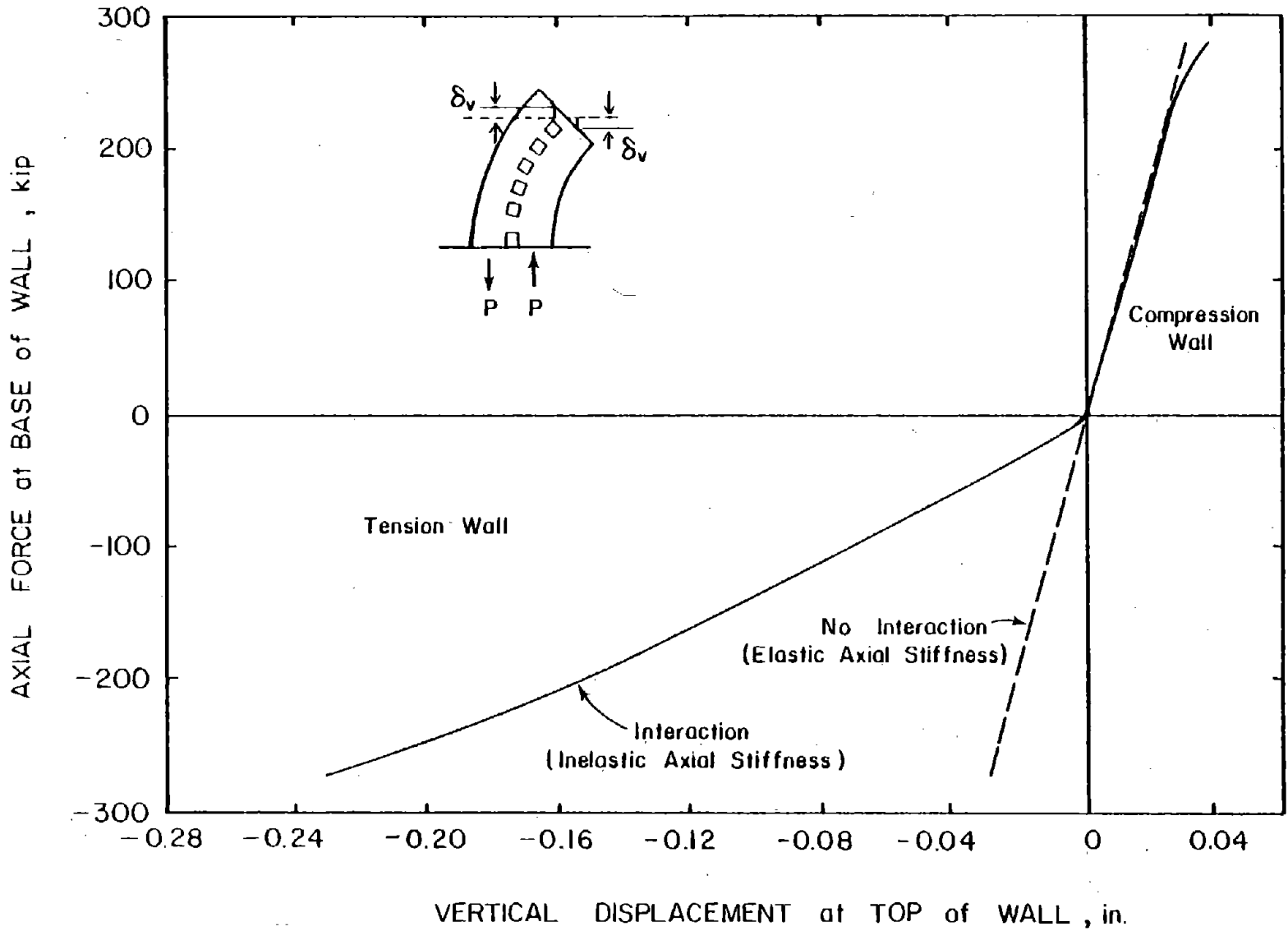
Relationship of CS-1

Fig. 7 Calculated Axial-Force-Versus-Vertical-Displacement
Relationship of RCS-1

As shown in Fig. 6, Specimen CS-1 exhibits a significant reduction in axial stiffness for the tension wall as well as for the compression wall as loads increase. The maximum top vertical displacement of the tension wall including the interaction effect is about 6 times as much as the elastic response value. The corresponding value for the compression wall is about 4 times. Curves for both the tension and compression walls indicate a small coupling effect for the specimen.

On the other hand, in the case of Specimen RCS-1, the tension wall curve is significantly different from that for the compression wall as shown in Fig. 7. The curve for the tension wall is softened markedly once flexural cracks open at a very early stage of loading. The maximum top vertical displacement of the tension wall, for the case where the interaction effect is included, is about 6 times as large as it would be if the axial stiffness of the wall remained elastic.

For the compression wall, the curves for inelastic axial stiffness and for elastic axial stiffness show practically no difference. This means that, if compressive forces due to the coupling effect are large enough to offset the opening of flexural cracks, the compression wall can be assumed to behave elastically in the axial direction.

Redistribution of Base Shear in Two Walls. Figures 8 and 9 show the change in distribution of base shear between the two walls with increase in applied loads for Specimens CS-1 and RCS-1, respectively. A part of the shear force in the tension
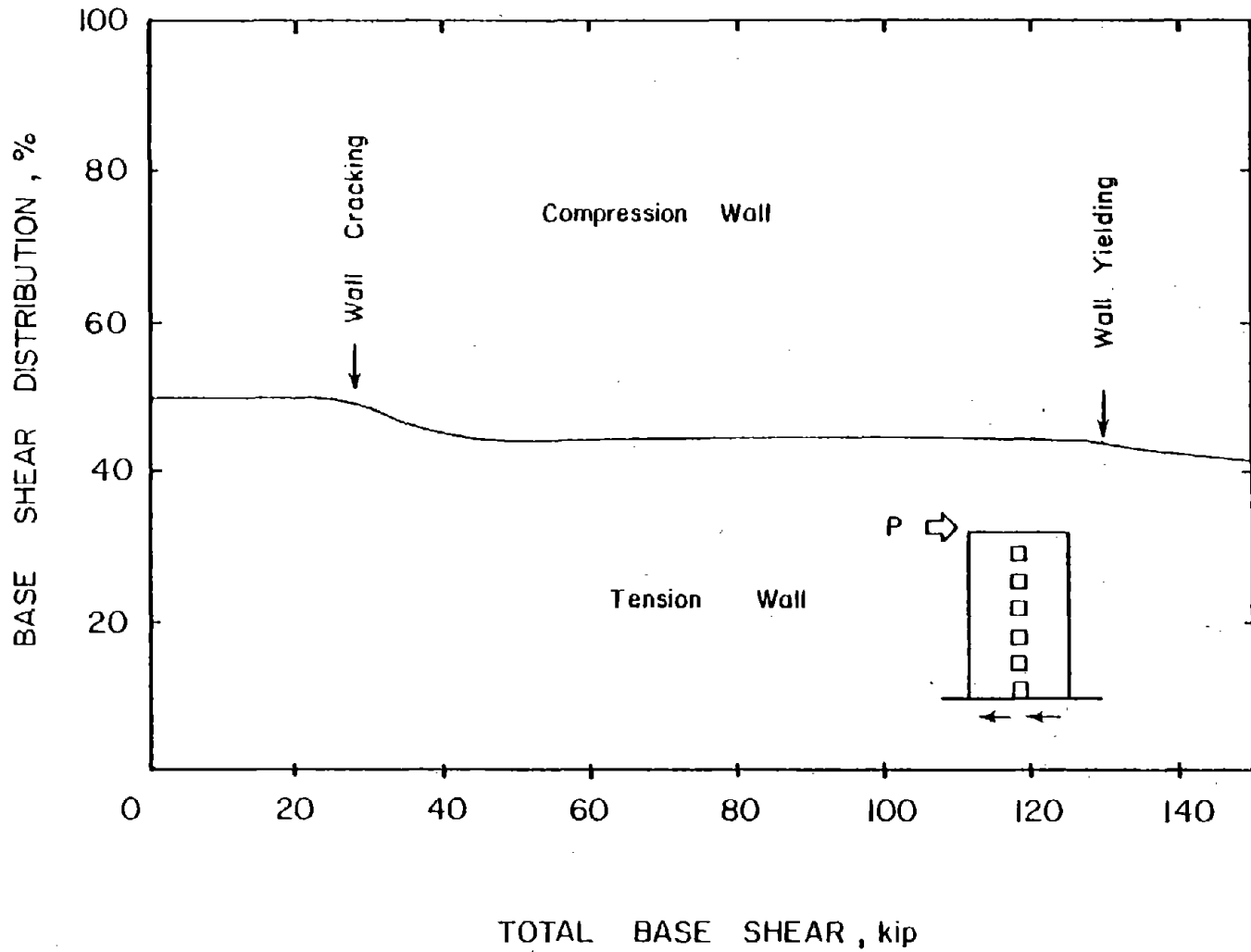
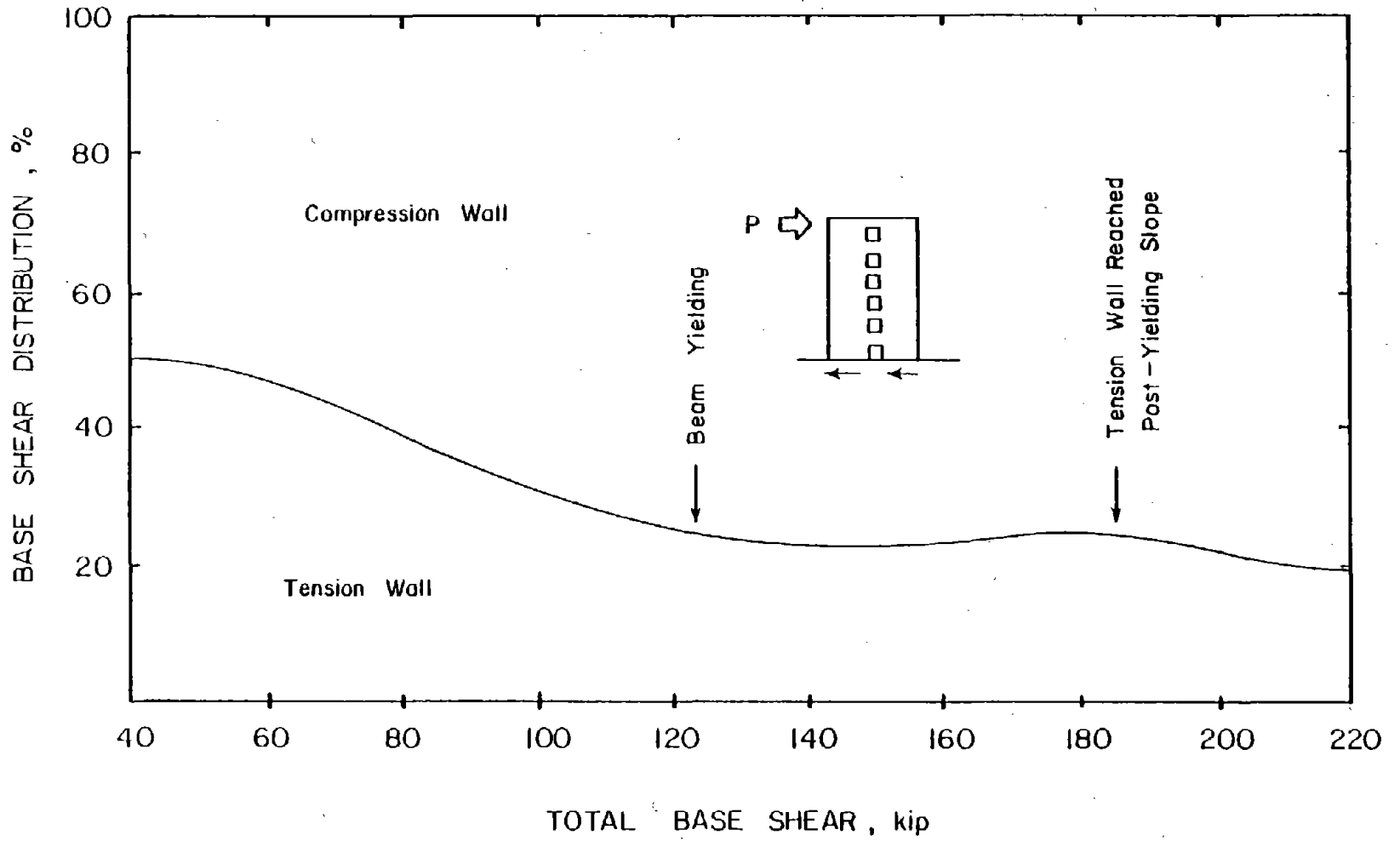Fig. 8   Calculated Shear Force Redistribution of CS-1

Fig. 9   Calculated Shear Force Redistribution of RCS-1

wall is transferred to the compression wall through the connect-
ing beams because of changes in wall flexural and shear stiff-
nesses.

Shear force transferred at each floor level is accumulated
down to the base. The transferred shear causes a compressive
force in the connecting beams so that the strength of the con-
necting beams increases. This is especially true for RCS-1. An
iteration process is adopted to include the effect of the beam
strength increase in the analysis of RCS-1. The iterative
process is as follows:

   (1) The flexural strength without the axial force effect is
       assumed for each connecting beam in the first run.

   (2) The flexural strength of each connecting beam is recal-
       culated based on the existing axial force recorded at
       the end of the first run.

   (3) The second run is implemented assuming a revised flex-
       ural strength for each connecting beam. Calculated
       results of the second run are used in the comparison
       with experimental results.

As shown in Fig. 8, the base shear of CS-1 is equally dis-
tributed between the two walls in the elastic range. When
cracking in the tension wall is initiated, the base shear in the
tension wall starts shifting to the compression wall. At maxi-
mum load, 43% of the total base shear is taken by the tension
wall.

For Specimen RCS-1, the transfer of shear is more signifi-
cant. At maximum load, only 20% of the total base shear is

-28-

carried by the tension wall while the remaining portion is taken by the compression wall.

It was assumed that the two walls of RCS-1 were equally damaged as a result of the CS-1 test. Therefore, the same initial stiffness was used for each wall.

Coupling Effect in Lateral Deflection. Coupling action of the two walls connected through the beams is one of the most distinctive features of the coupled wall system. The lateral deflection at the top floor level consists of flexural and shear components of deformation of the individual walls in addition to story rotation due to contraction of the compression wall and elongation of the tension wall.

The contribution of story rotation to the top lateral deflection is an indicator of the magnitude of the coupling effect. The ratio of the deflection due to the coupling effect to the total deflection is used to indicate the significance of this coupling effect. This ratio keeps changing during the process of loading reflecting inelastic actions taking place in the constituent elements.

Variations in ratios at successive levels of deflection for CS-1 and RCS-1 are shown in Figs. 10 and 11, respectively. As shown in these figures, the ratios start to change whenever inelastic events, such as concrete cracking or reinforcement yielding at critical parts of the constituent members take place.

For CS-1, the initial ratio of 27% reduces to 20% at cracking of the walls and beams. After reaching 20%, the ratio

δc = Top Story Deflection due to Coupling Behavior of Two Walls

δ_T = Total Top Story Deflection

δ_{c2} = Top Deflection due to 2nd Story Rotation, θ_2

$$\delta c = \sum_{n=1}^{6} \delta cn$$
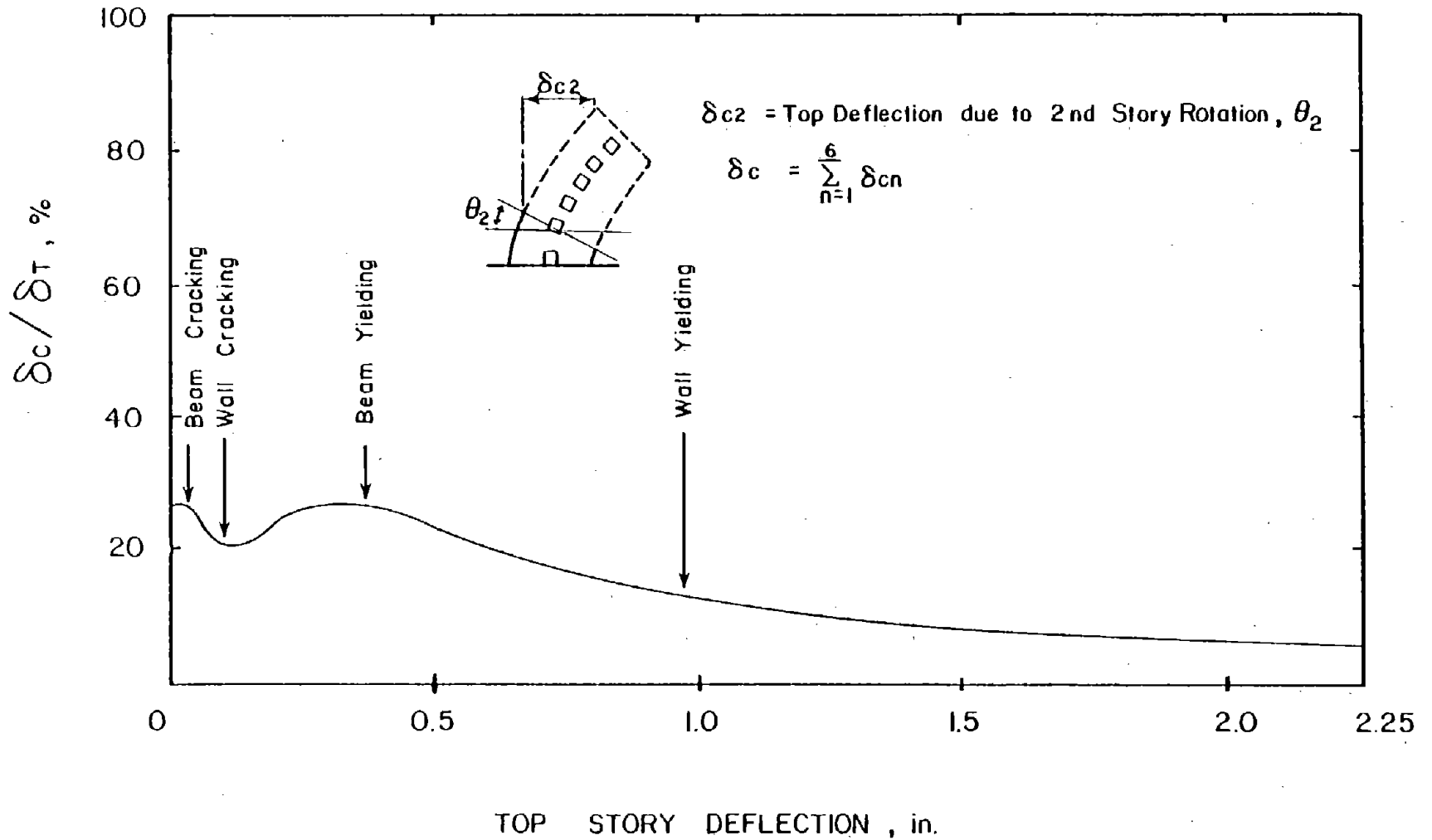
Fig. 10   Coupling Effect in Calculated Lateral Deflection of CS-1

δ_c = Top Story Deflection due to Coupling Behavior of Two Walls

δ_T = Total Top Story Deflection

Beam Cracking

Beam Yielding

Tension Wall Reached Post-Yielding Slope

Compression Wall Reached Post-Yielding Slope

δ_{c2}

θ_2

δ_{c2} = Top Deflection due to 2nd Story Rotation, θ_2

$$\delta_c = \sum_{n=1}^{6} \delta_{cn}$$

TOP STORY DEFLECTION, in.

Fig. 11 Coupling Effect in Calculated Lateral Deflection of RCS-1

gradually starts to increase until beam yielding occurs as shown
in Fig. 10. During increase of the ratio, the wall axial stiff-
ness decreases faster than flexural stiffness. When yielding of
the connecting beams starts, the ratio starts decreasing again
and continues this trend to the end of loading. No significant
increase of axial force in the walls occurs at this stage. The
ratio ranges from 27% at the beginning stage to 6% at the final
stage and indicates relatively light coupling in CS-1.

As shown in Fig. 11, RCS-1 shows a much greater coupling
effect than CS-1. The initial ratio of 65% gradually decreases
to 60% when yielding of the connecting beams starts. After
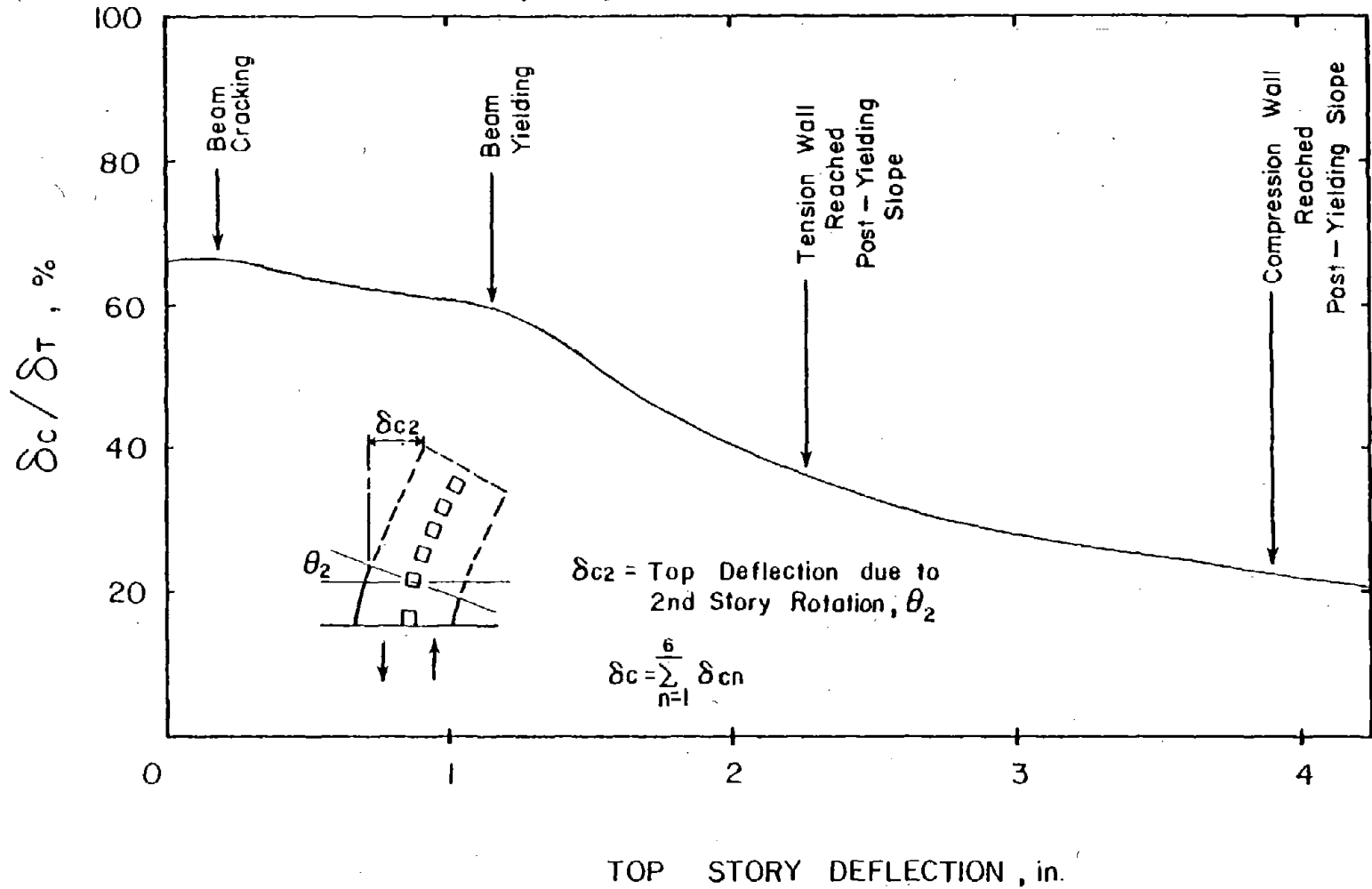yielding in the beams the ratio decreases at a faster rate. The
ratio eventually decreases to 20% at the end of loading. These
results for RCS-1 show that a significant portion of the lateral
deflection is caused by coupling action even late in the loading
sequence when large deflections occur.

Base Moment Distribution Pattern. Overturning moment at
each story level is resisted by the coupling moment due to the
axial forces in the walls and the flexural moments in the indi-
vidual walls. The ratio of coupling moment to overturning
moment at the base is another indicator of the relative magni-
tude of the coupling effect with respect to the total behavior
of coupled wall systems.

Variations in the coupling moment to overturning moment
ratio with increasing load for CS-1 and RCS-1 are illustrated
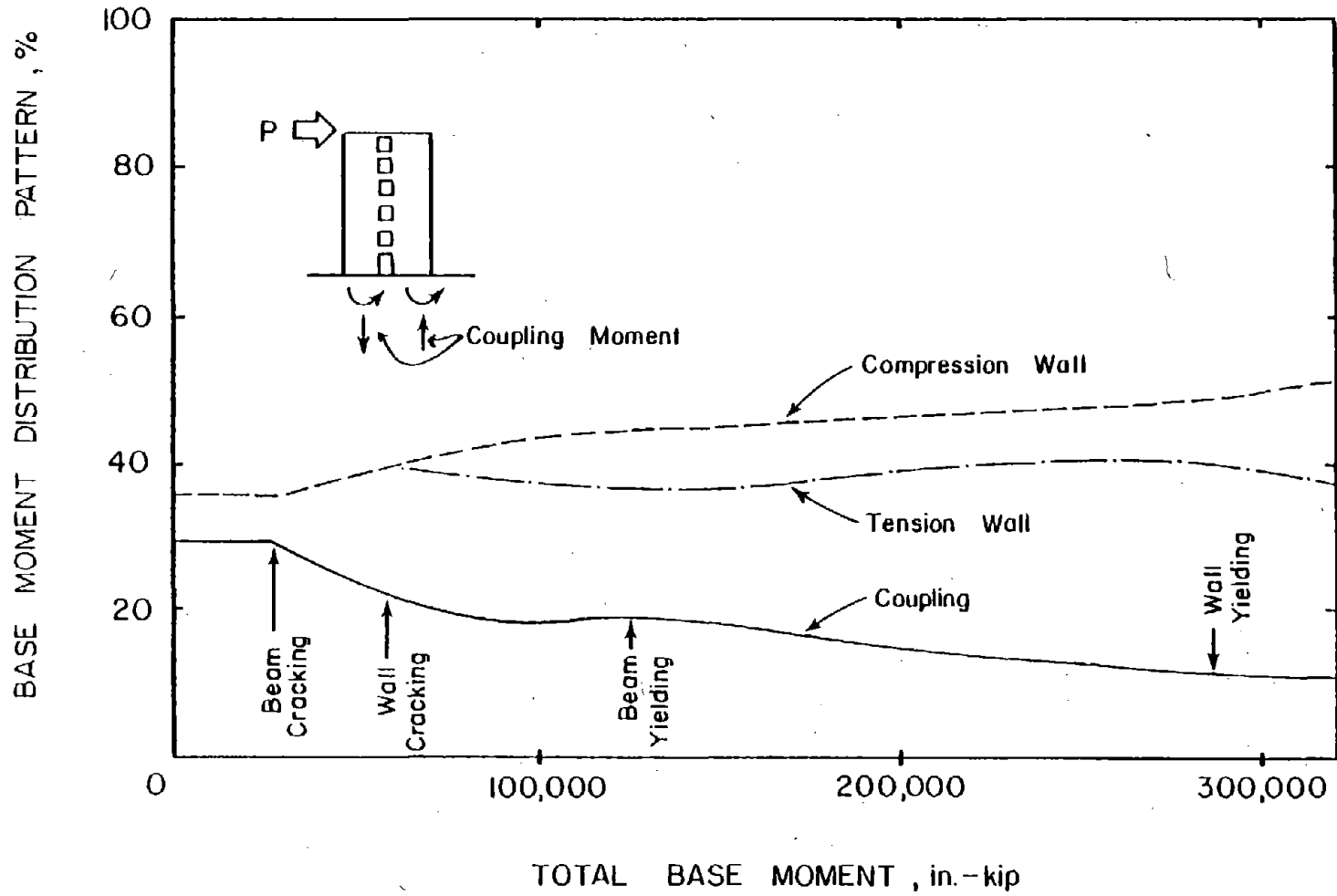in Figs. 12 and 13, respectively. Also shown in the same

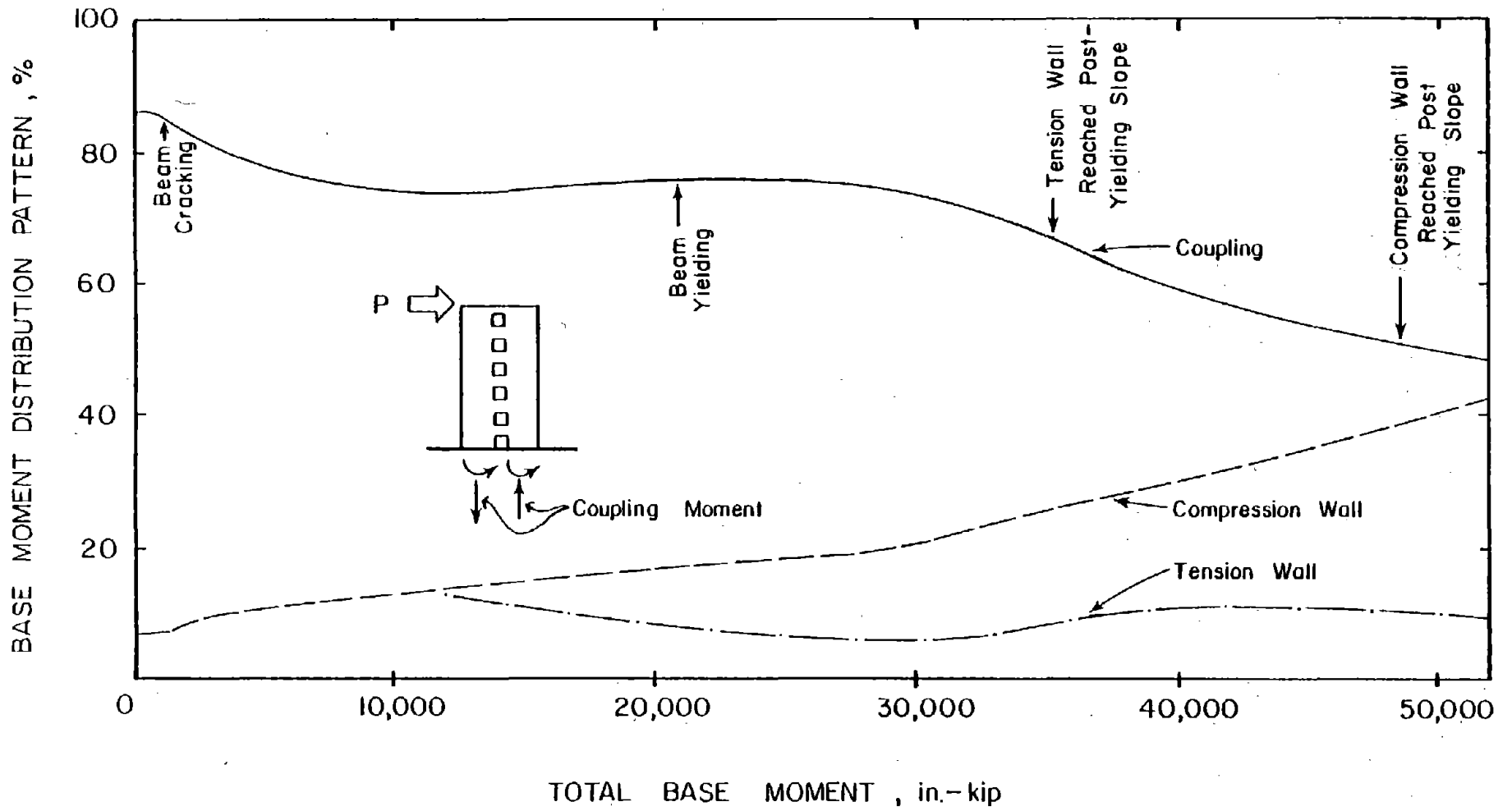Fig. 12   Calculated Base Moment Distribution Pattern of CS-1

Fig. 13   Calculated Base Moment Distribution Pattern of RCS-1

figures are variations in the ratios of flexural moments in the compression and tension walls to overturning moment. Change in the ratios as loading increases indicates inelastic action taking place in critical members.

For CS-1, the ratio of coupling moment to overturning moment starts at about 30% as shown in Fig. 12. This ratio indicates relatively light coupling for the specimen. The ratio starts decreasing when cracking occurs in the beams. This decreasing trend is moderated at the initiation of cracking in the walls. The ratio starts decreasing again when yielding of beams occurs. This decrease continues up to the initiation of yielding in the walls when the ratio reduces to 12%. Inelastic behavior in the connecting beams is a major contributor to the decreasing trend of the ratio.

Calculated results for RCS-1 show the same tendency as for CS-1 except in the magnitude of the coupling ratio. As shown in Fig. 13, the ratio of coupling moment to overturning moment starts at 85% indicating a large coupling of the two walls connected by strong beams. The ratio starts decreasing when inelastic action in the members takes place. Inelastic action of the connecting beams, such as cracking of concrete and yielding of reinforcement, accelerates this decreasing rate. At the end of loading, the coupling moment accounts for 50% of the overturning moment at the base.

The remaining portion of the overturning moment is the sum of the flexural moment in the compression wall and that in the tension wall. This flexural moment is equally distributed

between the compression wall and the tension wall at the beginning of loading. As inelastic action takes place in the walls, the tension wall starts decreasing its share of the flexural moment. For CS-1, the contribution of the tension wall represents about 42% of the total flexural moment at the end of loading as shown in Fig. 12. This shows that a small amount of the flexural moment has shifted from the tension wall to the compression wall.

On the other hand, the tension wall of RCS-1 shares only 20% of the total flexural moment at the end of loading as shown in Fig. 13. A large amount of the flexural moment has shifted from the tension wall to the compression wall during the loading process. The shift of flexural moment reflects early deterioration in the tension wall, prior to deterioration in the compression wall.

Load-Versus-Top-Floor-Displacement Relationship Under Reversed Loading. Figure 14 shows the load-deflection relationships of CS-1 under reversed loading. Yielding sequence of constituent members is also shown. Although the calculated curve slightly underestimates the absorbed energy relative to the observed curve in the test, the analytical result satisfactorily predicts the test result.

In the analysis, pinching behavior in the moment-rotation relationship of the beams was based on results of beam element tests. However, no significant pinching effect is exhibited in either the analytical result or the experimental results.
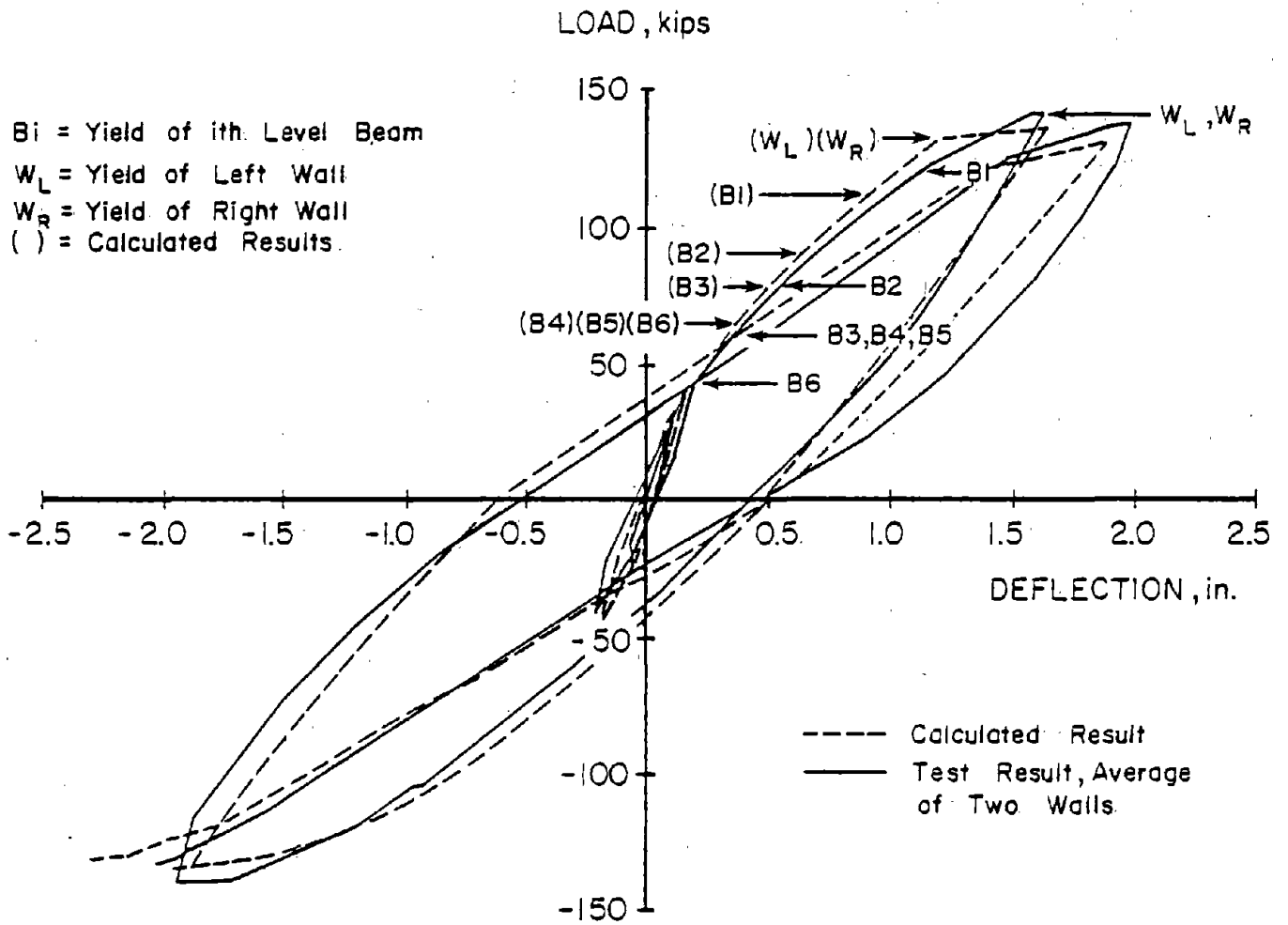
Fig. 14   Load-Versus-Top-Floor-Deflection Relationship
of CS-1 Under Reversed Loading

Absence of significant pinching can be attributed to weak connecting beams used for this specimen.

A corresponding analysis for RCS-1 was not attempted, because the hysteresis rules built into the computer program are not applicable to a structure already damaged before loading.

SUMMARY AND CONCLUSIONS

A structural model that can predict the response history and failure mechanisms of coupled wall systems under static load is described in this report. The model was applied to coupled wall specimens tested at the Construction Technology Laboratories.

The analytical results are compared with test results. Effects of assumed analytical conditions on overall behavior of the structures are discussed on the basis of this comparison.

Conclusions drawn from the analysis of coupled wall systems and the comparison of analytical results with test results are:

1. Analytical models used in this investigation can simulate important aspects of behaviour of constituent members of coupled wall systems.

2. The analytical results are in satisfactory agreement with the experimental results with respect to overall behavior of the coupled wall systems considered.

3. For a two-wall system coupled by weak beams, the individual walls govern overall behavior of the system. Inelastic shear deformation in walls plays a significant role in reducing the system stiffness as loading increases.

4. In the heavily coupled wall system, RCS-1, a large amount of the shear is transferred to the compression wall through connecting beams. As a result, the compression wall shares larger portions of the shear and moment at its base relative to the tension wall. To reproduce the concentration of shear and moment in

the compression wall, interaction between axial and flexural actions in the walls should be included in the analysis.

5. RCS-1 is characterized by heavy coupling between the two walls. At the initial stage of loading 85% of the base moment is taken by the coupling moment. For CS-1, with relatively light coupling beams, only 30% of the base moment is taken by the coupling moment at initial loading.

ACKNOWLEDGEMENTS

REFERENCES

1. Hognestad, E., "A Study of Combined Bending and Axial Load in Reinforced Concrete Members," University of Illinois Engineering Experimental Station, Bulletin Series No. 399, November 1951.

2. Ma, S.M., Bertero, V.V. and Popov, E.P., "Experimental and Analytical Studies on the Hysteretic Behavior of Reinforced Concrete Rectangular and T-Beams," EERC Report No. 76-2, University of California, Berkeley, May 1976.

3. ACI Committee 318, Building Code Requirements for Reinforced Concrete, ACI Standard 318-77, American Concrete Institute, Detroit, Michigan, 1977.

4. Hirosawa, M., Past Experimental Results on Reinforced Concrete Shear Walls and Analysis on Them, Kenchiku Kenkyu Shiryo No. 6, Building Research Institute, Ministry of Construction of Japan, March 1975 (in Japanese).

5. Arakawa, T., "Allowable Unit Shearing Stress and Design Method of Shear Reinforcement of Reinforced Concrete Beams," Concrete Journal, Japan National Council on Concrete, Vol. 8, No. 7, July 1970 (in Japanese).

6. Shibata, T., "Ultimate Strength Equations of Reinforced Concrete Members at Brittle Failure," Concrete Journal, Japan Concrete Institute, Vol. 18, No. 1, January 1980 (in Japanese).

7. Oesterle, R.G., Fiorato, A.E., Johal, L.S., Carpenter, J.E., Russell, H.G. and Corley, W.G., "Earthquake-Resistant Structural Walls - Tests of Isolated Walls," Report to the National Science Foundation, Portland Cement Association, November 1976.

8. Takayanagi, T. and Schnobrich, W.C., "Computed Behavior of Reinforced Concrete Coupled Shear Walls," Structural Research Series No. 434, Civil Engineering Studies, University of Illinois, December 1976.

9. Oesterle, R.G., Fiorato, A.E., Aristizabal-Ochoa, J.D. and Corley, W.G., "Hysteretic Response of Reinforced Concrete Structural Walls," submitted for publication in the ACI Symposium Volume on Mathematical Modeling of Reinforced Concrete Structures, Toronto, 1978.

10. Otani, S. and Sozen, M.A., "Behavior of Multistory Reinforced Concrete Frames during Earthquakes," Structural Research Series, No. 392, Civil Engineering Studies, University of Illinois, Urbana, November 1972.

REFERENCES (CONTD.)

11. Takeda, T., Sozen, M.A. and Nielsen, N.N., "Reinforced Con-
    crete Response to Simulated Earthquakes," Journal of the
    Structural Division, ASCE, Vol. 96, No. ST12, December 1970,
    pp. 2,557-2,573.

12. Shiu, K.N., Aristizabal-Ochoa, Barney, G.B., Fiorato, A.E.,
    and Corley, W.G., "Earthquake Resistant Structural Walls -
    Coupled Wall Tests," Report to the National Science Founda-
    tion, Portland Cement Asssociation, July, 1981.

13. Barney, G.B., Shiu, K.N., Rabbat, B.G., Fiorato, A.E.,
    Russell, H.G., and Corley, W.G., "Earthquake Resistant
    Structural Walls - Tests of Coupling Beams," Report to the
    National Science Foundation, Portland Cement Association,
    Skokie, January 1978.

14. Shiu, K.N., Daniel, J.I., Aristizabal-Ochoa, J.D., Fiorato,
    A.E., and Corley, W.G., "Earthquake Resistant Structural
    Wall Systems - Pierced Wall Test," Report to the National
    Science Foundation, Portland Cement Association, Skokie.
    (to be published).

APPENDIX A - DEVELOPMENT OF MEMBER ANALYTICAL MODELS

Procedures used in developing the analytical models for constituent members are explained in this Appendix. Force-deformation relationships for members are derived from stress-strain relationships of the constituent materials. In addition, hysteresis rules adopted for different types of members are discussed in detail.

Material Properties

Inelastic sectional properties of member elements are based on idealized stress-strain curves for concrete and reinforcement. Moment-curvature and axial force-axial strain relationships of a section are developed by integrating stress distributions over the section. Stress distributions are determined based on the assumption of linear variation in strain across the cross section.

Stress-Strain Relationship of Concrete.

A parabola combined with a straight line as proposed by Hognestad[1] is adopted for the stress-strain relationship of concrete. The relationship is:

$$f_c = 0 \qquad\qquad \varepsilon_c \leq \varepsilon_t$$

$$f_c = f'_c \left[2\left(\frac{\varepsilon_c}{\varepsilon_o}\right) - \left(\frac{\varepsilon_c}{\varepsilon_o}\right)^2 \right] \qquad \varepsilon_t \leq \varepsilon_c \leq \varepsilon_o \qquad (A1)$$

$$f_c = f'_c \left[1 - Z(\varepsilon_c - \varepsilon_o) \right] \qquad\qquad \varepsilon_o \leq \varepsilon_c$$

and

$$\varepsilon_t = \varepsilon_o \left[1 - (1 - f_c/f_c')^{\frac{1}{2}} \right] \qquad (A2)$$

$$f_t = -6.0 \ (f_c')^{\frac{1}{2}} \qquad (A3)$$

where

f_c = concrete stress

f_c' = uniaxial compressive strength of concrete

f_t = tensile strength of concrete

ε_c = concrete strain

ε_o = strain at f_o'

ε_t = strain at f_t

Z = constant defining the descending slope
of the stress-strain curve. A value of
100 was used in the analysis.

The adopted curve is shown in Fig. A1.

Stress-Strain Relationship of Reinforcement. A piecewise
linear stress-strain relationship is adopted for the reinforce-
ment. The relationship is:

$$
\begin{aligned}
f_s &= E_s \ \varepsilon_s & \varepsilon_s &\leq \varepsilon_y \\
f_s &= f_y & \varepsilon_y &\leq \varepsilon_s \leq \varepsilon_h & (A4) \\
f_s &= f_y + E_h \ (\varepsilon_s - \varepsilon_h) & \varepsilon_h &\leq \varepsilon_s \leq \varepsilon_u \\
f_s &= f_u & \varepsilon_u &- \varepsilon_s
\end{aligned}
$$

where

f_s = reinforcement stress

f_y = yield stress of the reinforcement

f_u = ultimate stress of the reinforcement

ε_s = strain of the reinforcement

ε_y = strain at f_y

ε_h = strain at onset of strain hardening

ε_u = strain at f_u

E_s = modulus of elasticity of the reinforcement

E_h = modulus to define stiffness in strain
hardening range

The proposed stress-strain curve for reinforcement is illustrated in Fig. A2. The relationship is assumed to be symmetric with respect to the origin.

Sectional Properties

Member stiffness is obtained by integrating sectional properties over the length of the member. Each sectional property can be expressed by either analytically developed equations based on the material properties or empirical equations based on a number of tests.

Moment-Curvature Relationship. The primary moment-curvature curve of a section subjected to a monotonically increasing moment and a constant axial force can be derived based on the idealized material properties of concrete and reinforcement. It is assumed that strain varies linearly over the depth of the section as shown in Fig. A3. Curvature and strains are related through the following equations.
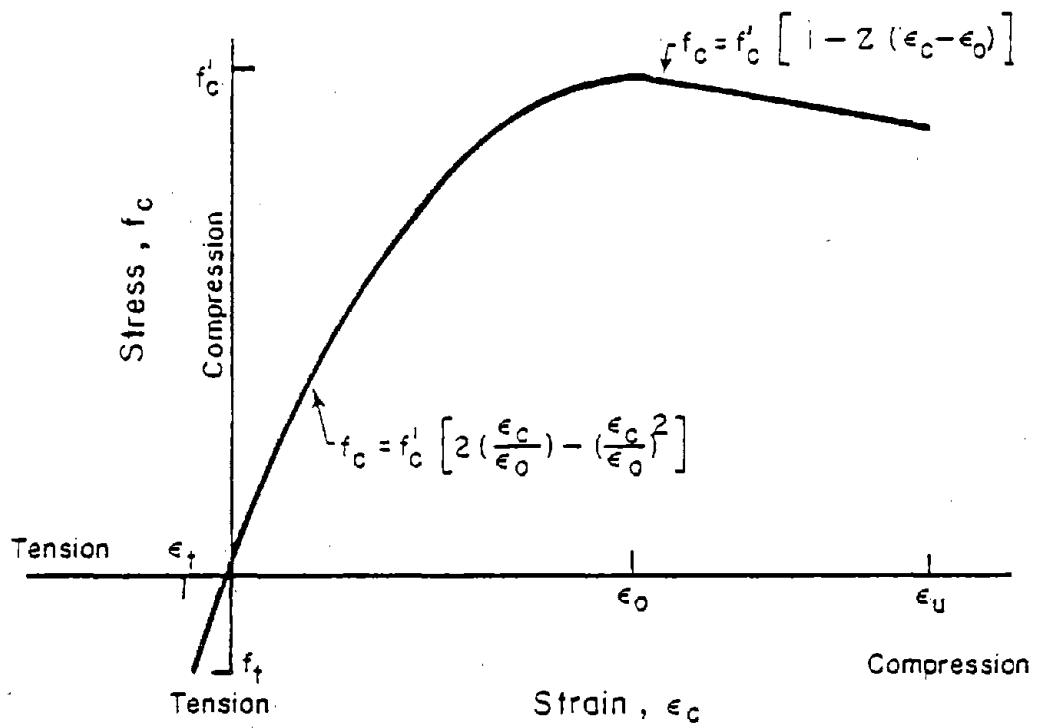
Fig. A1   Idealized Stress-Strain Relationship of Concrete

Where the upper curve is labeled:

$$f_c = f_c' \left[1 - Z (\epsilon_c - \epsilon_0) \right]$$

and the lower curve is labeled:

$$f_c = f_c' \left[2 \left(\frac{\epsilon_c}{\epsilon_0} \right) - \left(\frac{\epsilon_c}{\epsilon_0} \right)^2 \right]$$

Fig. A2   Idealized Stress-Strain Relationship of Reinforcement

A-4
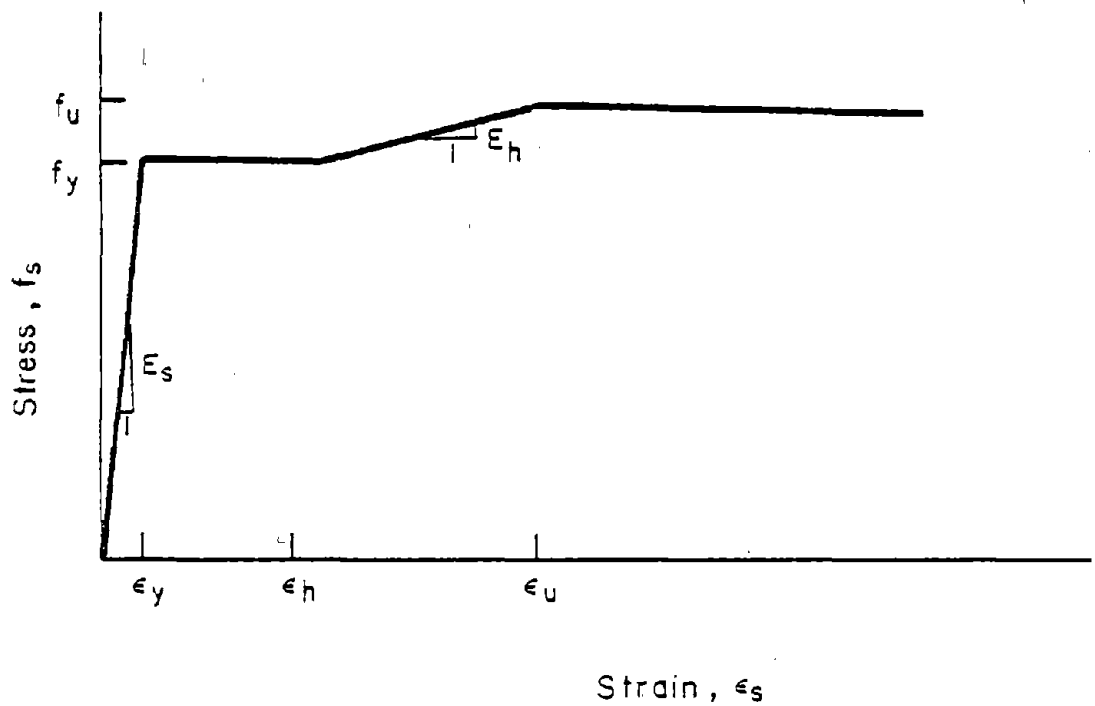
(a) Cross Section   (b) Strain Distribution   (c) Stress Distribution
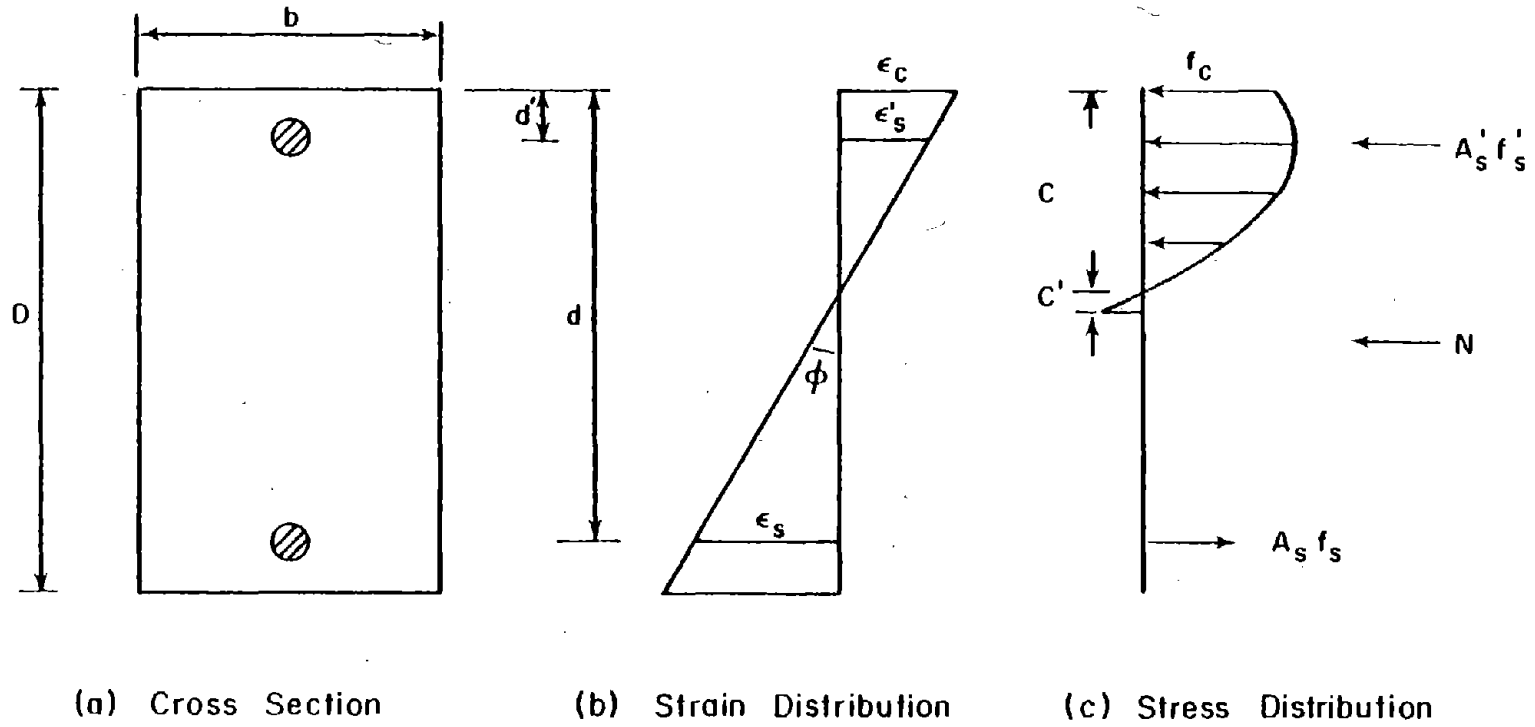
Fig. A3   Distributions of Stress and Strain
Over a Cross Section

$$\Phi = \varepsilon_c/c$$
$$= \varepsilon_s'/(c - d') \tag{A5}$$
$$= \varepsilon_s/(d - c)$$

where

Φ = curvature

ε_c = concrete strain at extreme compressive fiber

ε_s' = strain in compressive reinforcement

ε_s = strain in tensile reinforcement

d' = distance from extreme compressive fiber

to center of compressive reinforcement

d = distance from extreme compressive fiber to

center of tensile reinforcement

c = depth of neutral axis

Equilibrium of resultant forces results in the following expression.

$$\int_{-c'}^{c} f_c b \, dx + A_s' f_s' - A_s f_s = N \tag{A6}$$

where

f_s' = stress in compressive reinforcement

f_s = stress in tensile reinforcement

b = width of cross section

A_s' = total area of compressive reinforcement

A_s = total area of tensile reinforcement

N = axial load acting on section

c' = distance from neutral axis to point of maximum

tensile stress in concrete

Resultant moment M, at depth x, can be calculated by the following equation.

$$M = \int_{-c'}^{c} f_c b \zeta d\zeta + (x - c)\int_{-c'}^{c} f_c b dx + A_s' f_s' (x-d')$$

$$+ A_s f_s (d - x) + N (x - \frac{D}{2}) \tag{A7}$$

where

D = total depth of section

ζ = distance from neutral axis

The first term on the right-hand side of Eq. A7 represents the moment due to the concrete stress block calculated with respect to the neutral axis. The second term reflects the change of the moment axis location from the neutral axis to the depth, x. Normally, the moment, M, is evaluated with respect to the plastic centroid of the section.

An iterative method is used to solve Eqs. A5 and A6 for c with given Σ_c and N. The moment, M, and curvature, Φ, can be derived by Eqs. A5 and A7 with calculated c and given $_c$. Moment-curvature curves for a wall section subjected to different axial forces, calculated on the basis of the abovementioned procedure, are shown in Fig. A4.

For simplicity, the original moment-curvature curves are trilinearized. The slopes in the three stages of this idealized moment-curvature relationship are defined as follows:
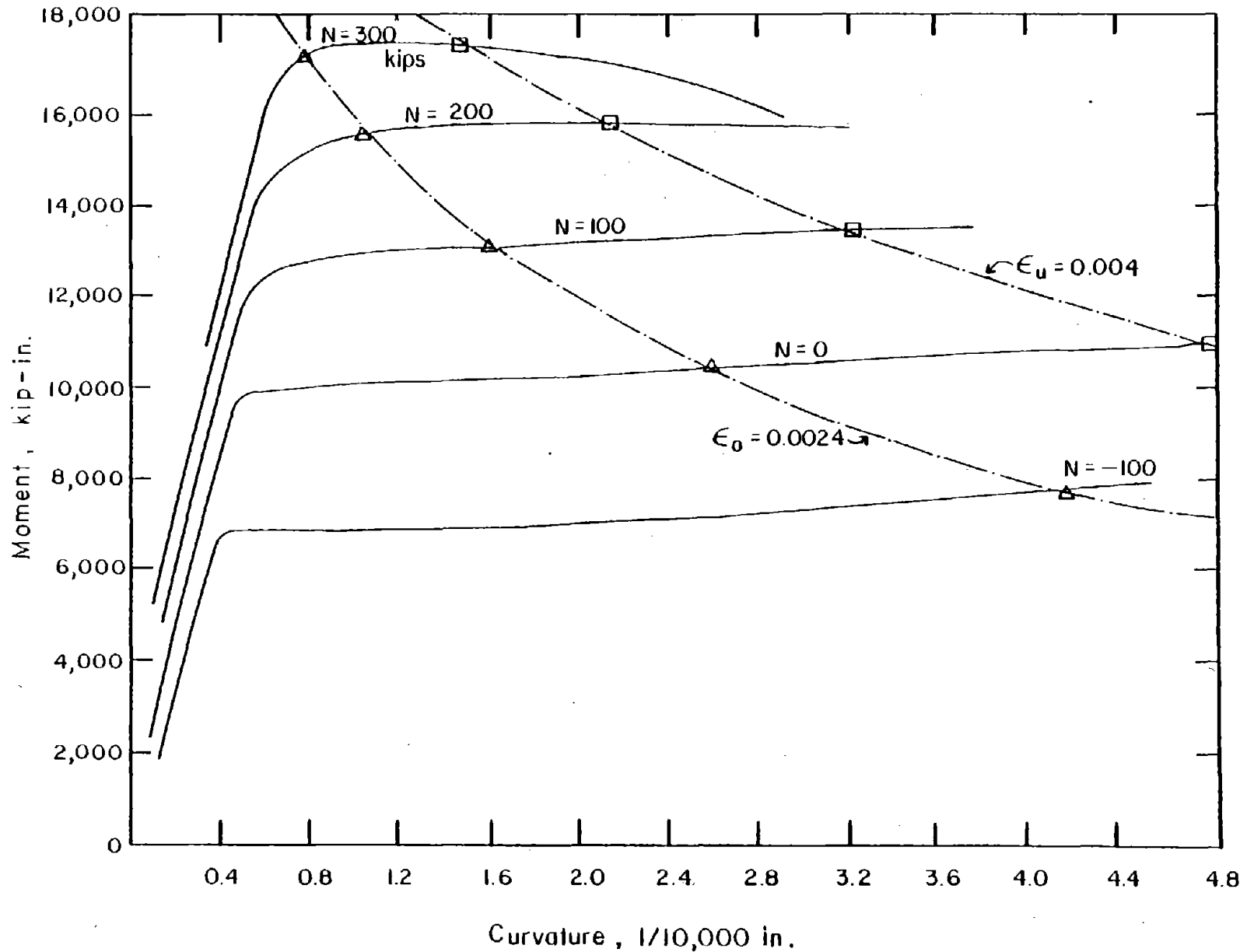
Fig. A4 Moment-Versus-Curvature Curves for Different Axial Force

$$\Phi = M / \frac{\frac{M_c}{}}{\Phi_c} \qquad\qquad M \leq M_c$$

$$\Phi = M / \frac{M_y - M_c}{\Phi_y - \Phi_c} + \Phi_c \qquad\qquad M_c \leq M \leq M_y \qquad\qquad \text{(A8)}$$

$$\Phi = M / \frac{M_u - M_y}{\Phi_u - \Phi_y} + \Phi_c \qquad\qquad M_y \leq M$$

where

M = bending moment

M_c = cracking moment

M_y = yielding moment

M_u = ultimate moment

Φ = curvature

Φ_c = curvature at cracking

Φ_y = curvature at yielding

Φ_u = curvature at ultimate stage

Cracking moment corresponds to the commencement of flexural cracking. Flexural cracking at a cross section occurs when the stress at the extreme tensile fiber of the section exceeds the concrete tensile strength. Yield moment is defined as the moment at yield of the tensile reinforcement.

A series of idealized moment-versus-curvature relationships of a wall section for different values of constant axial force is shown in Fig. A5.

Fig. A5   Idealized Moment-Versus-Curvature Relationships

<u>Axial-Force-Versus-Axial-Strain Relationship</u>.   The axial-
force-versus-axial-strain relationship of a section may be sig-
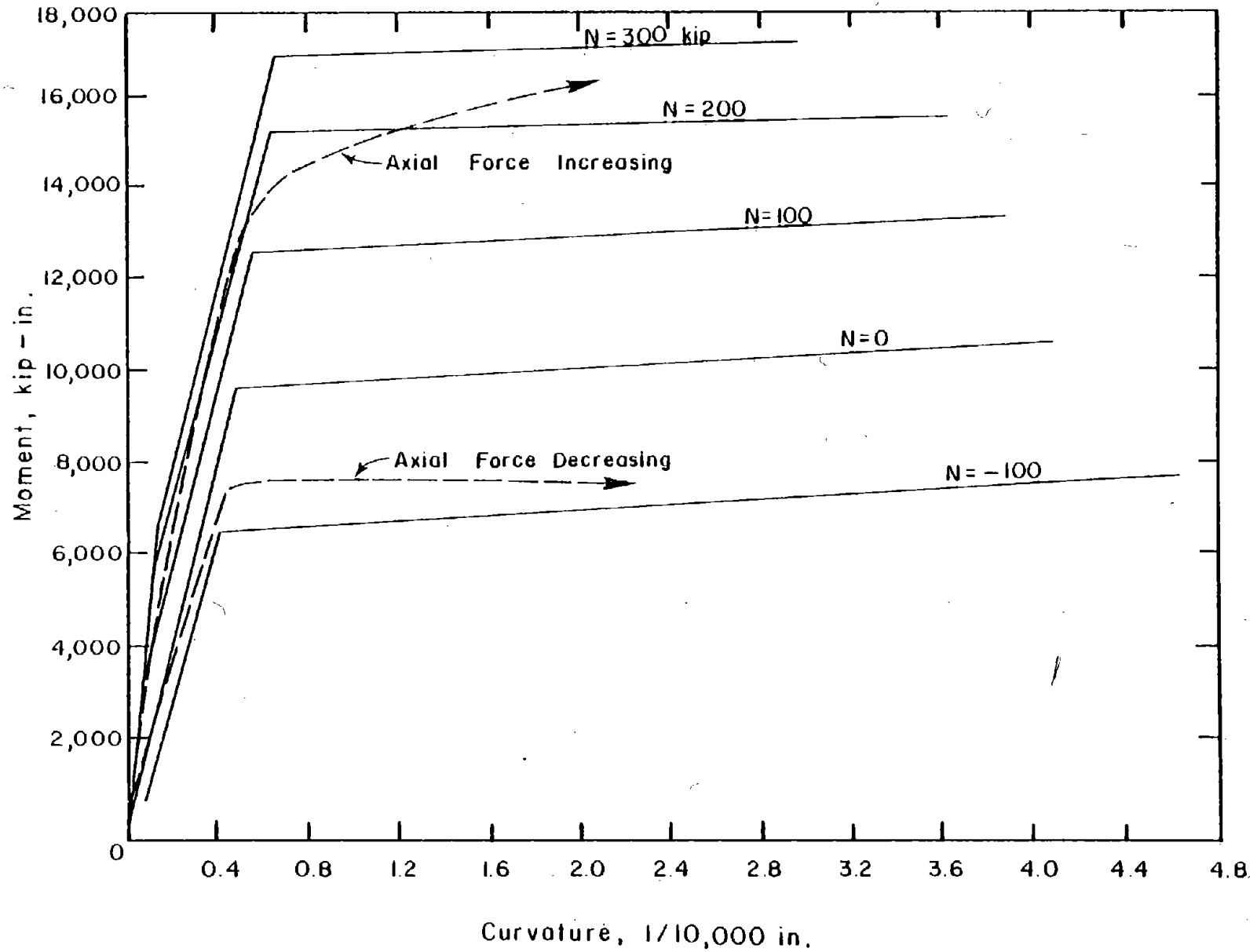nificantly affected by the presence of curvature in the section.
Therefore, an axial force-axial strain curve can be defined only
for a fixed curvature.   The axial-force-versus-axial-strain
relationship correspnding to a given curvature can be calculated
using the same procedure as for the moment-curvature relation-
ship.

In the procedure, axial strain is determined by taking an
average of the axial strain distribution over the cross section
with given curvature and axial force.   There are an infinite
number of such axial force-axial strain curves corresponding to
different values of curvature.   A series of axial force-axial-
strain curves is shown in Fig. A6.

It is assumed that the relation among axial force, axial
strain, and curvature can be established irrespective of the
loading history.   Therefore, if the axial force and curvature
at any stage in a loading process are known, the corresponding
axial strain can be uniquely determined without knowing the
previous history of loading.

To simplify the problem, the axial force-axial strain curves
are represented by straight lines with different slopes as shown
in Fig. A7.   The range of axial force-axial strain curves is
limited by two boundary lines A and B.   If an axial force-axial
strain curve exceeds either boundary line A or B, the curve is
assumed to travel along the corresponding line A or B.   Line A
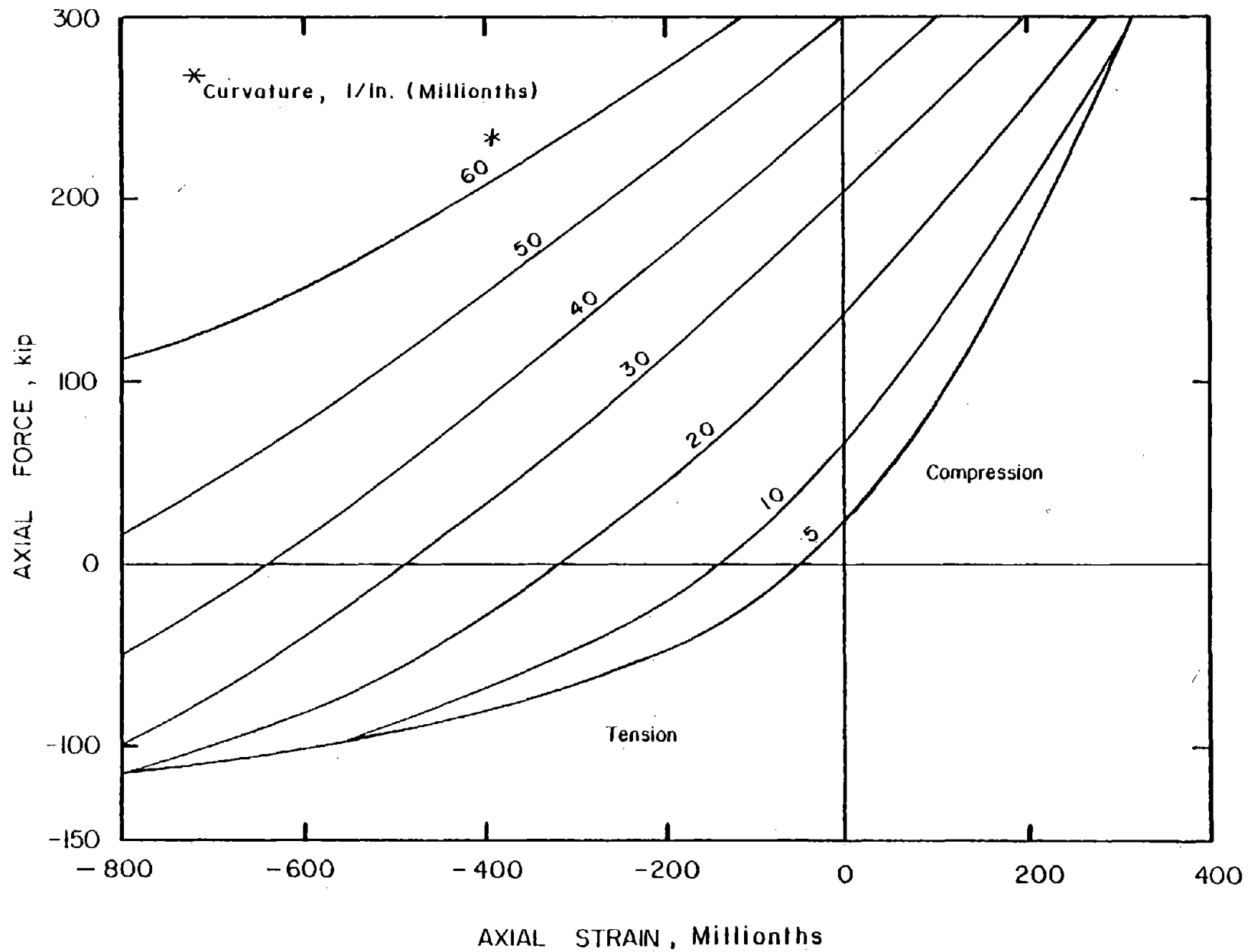corresponds to the situation where the tensile stress due to

Fig. A6   Axial-Force-Versus-Axial-Strain Curves for Different Curvatures
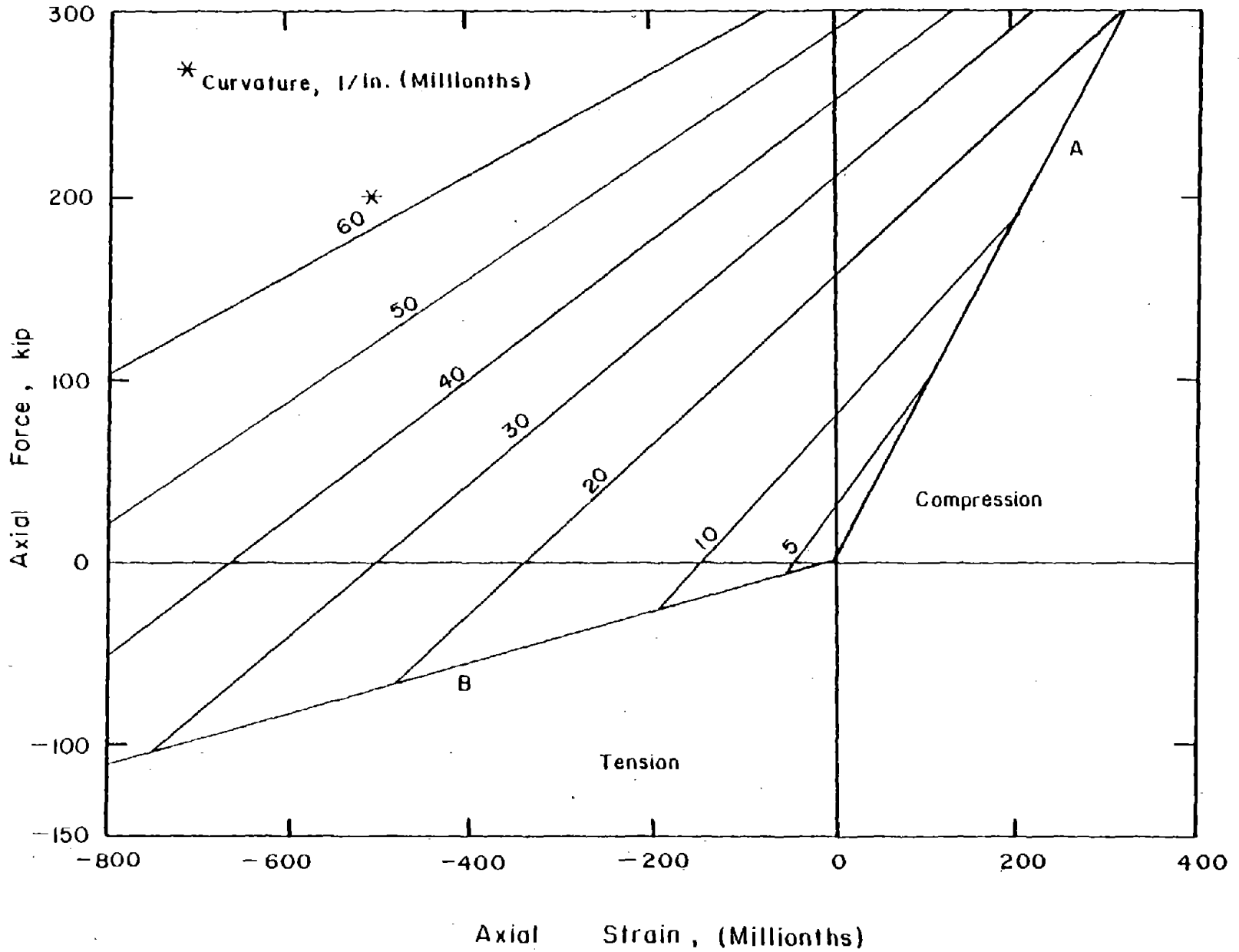
Fig. A7 Idealized Axial-Force-Versus- Axial Strain Relationships

moment is overcome by the compressive stress due to compressive force. Line B corresponds to a fully cracked section in which only reinforcing bars cary load. Line A is approximately straight until concrete crushing is initiated. Line B is straight until reinforcement yielding occurs.

Shear-Versus-Shear-Distortion Relationship. Development of a moment-curvature relationship for a section is straightforward from an analytical viewpoint. All quantities required for the moment-curvature relationship are defined at each section over the full loading range. The moment-curvature relationship can therefore be used to develop force deformation relationships for members idealized as line elements. However, it is difficult to establish the shear-versus-shear-distortion relationship for a section. The shear resistance mechanism is associated with inclined cracks that are not confined to a single section in the member. Therefore, the shear-versus-shear-distortion relationship can be evaluated only in an average sense over a length of the member.

There are two possible methods for evaluating parameters characterizing the primary curve for the shear-versus-shear-distortion relationship. One is to establish an elaborate model of the hinging region including detailed consideration of the various shear resisting mechanisms.[2] This would include such components as geometrical conditions associated with inclined shear cracking, flexural cracking and concrete struts, web reinforcement resistance, dowel action of reinforcement,

confinement of boundary elements, shear friction in the compression zone, bond degradation, and aggregate interlock. The primary curve of the shear-versus-shear-distortion relationship could then be evaluated by an analysis based on this elaborate model.

The other approach consists of modelling the gross or overall behavior of the hinging region. As with the first method, this approach relies heavily on experimental data.

At present, there is little data upon which to base a satisfactory model of inelastic shear behavior that would account for the contribution of various component mechanisms. This is true even for monotonic loading. The problems become even more complex in the case of reversed cyclic loading. In addition, such a model would be computationally very expensive for use in cyclic loading with no assurance of improvement in the accuracy of the results. Because of this, an approach based on total hinge behavior presently appears to be the most practical means of modelling inelastic shear behavior.

In order to establish the primary curve for the shear-versus-shear-distortion relationship, it is necessary to evaluate certain parameters. These parameters are cracking shear level, shear strength, and the corresponding shear distortions. An idealized primary curve for the shear-versus-shear-distortion relationsip is shown in Fig. A8.

The cracking shear level of wall members can be taken as the lesser of the results indicated by Eqs. (11-33) and (11-34) in Section 11.10.6 of the 1977 ACI Building Code (ACI 318-77).[3]
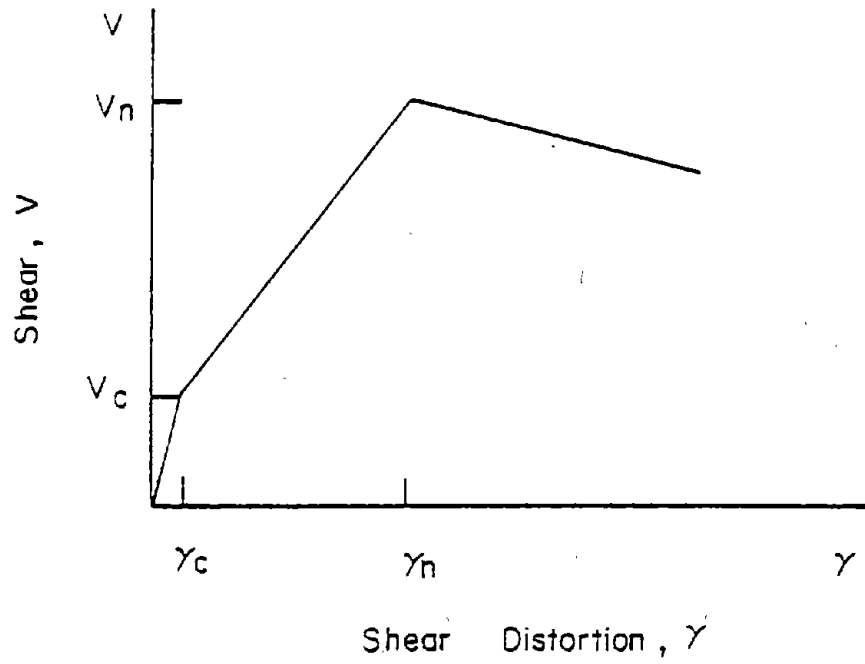
Fig. A8   Idealized Shear-Versus-Shear-Distortion Relationship

For the cracking level of beam members, Eq. (11-6) in Section 11.3.2 of ACI 318-77 can be used.

The shear strength of wall members can be roughly predicted by the following empirical equation[4].

$$V_n = \left\{ \frac{0.00371 \times \rho_f^{0.23}(f_c' + 2570)}{\frac{M}{V\ell_w} + 0.12} \right.$$

$$\left. + 0.0714 \sqrt{f_y \rho_h + 0.007 f_d} \right\} \qquad \text{(A9)}$$

$$\times h_e \left(\ell_w - \frac{h_c}{2} \right) \times 0.0124$$

where

h_e = average thickness of wall including boundary columns (in.)

ℓ_w = horizontal length of wall (in.)

h_c = depth of boundary column under tension (in.)

f_d = compressive stress of wall due to gravity load (psi)

ρ_h = horizontal web reinforcement ratio (%)

f_y = yield strength of web reinforcement (psi)

f_c' = compressive strength of concrete (psi)

ρ_f = ratio of main reinforcement area of column under tension to total area of wall (%)

M/V = moment-shear ratio (in.)

V_n = shear strength (kip)

This equation is based on a number of test results for isolated structural walls and accounts for the effect of the flexural

reinforcement in the boundary columns on the shear strength. No comparable expression relating shear capacity of walls with boundary columns is available in the ACI Code[3].

Furthermore, confinement of concrete in the adjacent columns, flexural moment capacity and failure mode might be considered as additional factors to evaluate the shear strength capacity of walls. These factors are not included in Eq. A9 and the ACI equations. Test results[4] indicate that the shear distortion corresponding to shear strength can be assumed equal to 0.003 radians for practical purposes.

The shear strength for beam members can be estimated by the following equation which is similar to the equation for wall members.[5]

$$V_n = \left\{ \frac{0.00384 \times \rho_f^{0.23}(f_c' + 2570)}{\frac{M}{Vd} + 0.12} + 0.0714 \sqrt{f_y \rho_h} \right\} bd \times 0.0124 \qquad (A10)$$

where

ρ_f = tensile reinforcement ratio (%)

f_c' = concrete strength (psi)

f_y = yield stress of shear reinforcement (psi)

ρ_h = shear reinforcement ratio (%)

M/V = moment versus shear ratio (in.)

V_n = shear strength (kip)

b = beam width (in)

d' = distance from extreme compression fiber to centroid of tensile reinforcement

Equation A9 for wall members is a modified version of Eq. A10.

The shear distortion corresponding to shear strength should be evaluated in order to establish the primary curve for the shear-versus-shear-distortion relationship. If the beam deflection corresponding to the shear strength is assumed to consist of flexural deflection and shear distortion, the shear distortion component in the total deflection can be roughly evaluated as the difference between the total deflection and the flexural deflection component. In view of the fact that the flexural deflection can be calculated by the sectional analysis reasonably accurately and the information as to the total deflection of beams is readily available in most tests results, values of shear distortion estimated in this procedure can be considered as being reasonably accurate.

Shibata claims in his paper[6] that Eq. A10 gives the smaller standard deviation than Eq. 11.2 of ACI 318-77 in terms of the ratio of test results to predicted values. Superiority of one equation over the other has not been clearly determined, however. Therefore, it was decided to use the lesser of values given by Eq. A9 and Eq. (11-2) of ACI for walls and the lesser of the results calculated by Eq. A10 and Eq. (11-2) of ACI 318-77 for beams.

Interaction Among Axial, Flexural and Shear Components

It appears reasonable to assume that for the general case, the instantaneous force-deformation relationships governing the axial, flexural and shear components in a member are inter-

related. This interrelationship becomes particularly signifi-
cant when structures behave inelastically under large load
reversals.

Simple analytical models have been developed in an attempt
to correlate these force components. Although three components,
axial, flexural and shear, are mutually interrelated in the
process of loading, only two types of interrelationship are
independently considered here. One is the interaction between
shear and moment and the other is the interaction between moment
and axial force. Other possible interactions such as shear and
axial force are ignored. However, shear and axial force are
indirectly correlated through the other two types of interrela-
tion considered here.

Coupling Between Shear and Moment. Instantaneous shear
distortion can be expressed as a function not only of shear
force but also of flexural rotation and axial deformation exist-
ing in a section as follows:

$$\gamma = \Gamma (V, \theta, \delta)$$ (A11)

in which V = shear force, θ = flexural rotation, and δ = axial
deformation. An incremental form of Eq. A11 is expressed as
follows:

$$d\gamma = \frac{\partial \Gamma}{\partial V} dV + \frac{\partial \Gamma}{\partial \theta} d + \frac{\partial \Gamma}{\partial \delta} d\delta$$ (A12)

At the present state of knowledge, it is difficult to eval-
uate the quantities on the right-hand side of Eq. A12 at any

instant in the process of loading. This is due mainly to the scarcity of experimental data and the lack of sufficient knowledge on the relationships among these quantities. But experimental results[2,7] clearly indicate that inelastic shear distortion is related to flexural yielding. The coupling is exhibited in the almost-simultaneous occurrence of shear yielding and flexural yielding well below the calculated shear capacity level.

Abrupt widening of flexural cracks and propagation of these cracks into the web at the onset of flexural yielding cause a change in shear resistance mechanism from truss analogy type to dowel action of vertical reinforcement and interface friction over the remaining small portion of compressive concrete.

Looking at this behavior from a different viewpoint, when shear cracks in the web are initiated, the wall starts to behave as an anisotropic material and tends to expand. However, this tendency is restrained by the boundary elements. After the boundary element reinforcement yields, this constraint is released causing a drastic reduction in shear stiffness. This phenomenon provides an explanation for the almost-simultaneous occurrence of flexural yielding and "shear yielding" observed in the tests of isolated walls conducted at the Construction Technology Laboratories.[7]

Generally shear distortion is related to flexural rotation in a complicated manner depending on the nominal shear stress level, size of flexural cracks, and other factors. A simple

analytical model was therefore established to reflect the basic inelastic shear mechanism identified experimentally.

In the analytical model, shear stiffness and flexural stiffness are combined in series. Interaction between shear distortion and flexural rotation is accounted for in the sense that, once either shear yielding or flexural yielding occurs, a reduction in element stiffness results. The shear force and moment are related through the equilibrium equations.

Interaction between shear yielding and flexural yielding can be incorporated into the inelastic shear-force-shear-distortion relationship in several ways.

The assumption that shear rigidity decreases in direct proportion to flexural rigidity was used in a previous study[8]. This assumption appears to be reasonable for members subjected to monotonically increasing loadings, since experimental results[9] indicate that the shear-distortion-flexural-rotation relationship is approximately linear even in the inelastic region.

The equation stating this assumption can be expressed in the form

$$GA_i = \frac{EI_i}{EI_e} GA_e \qquad (A13)$$

where

GA_i = inelastic shear rigidity

GA_e = elastic shear ridigity

EI_i = inelastic flexural rigidity

EI_e = elastic flexural rigidity

The mechanisms operating in pseudo-static tests where applied shear and moment are in phase produce shear and flexural deformations that are approximately linearly related.

However, this assumption may not be appropriate in dynamic response analysis. During dynamic response, the shear force and moment at a section are generally not in phase. Shear force usually varies much more rapidly than moment.

In the second approach the shear flexibility term in the member flexibility matrix is considered to be independent of the flexural flexibility term. Shear flexibility is assumed to be a function of only the shear and shear distortion. The shear yield level is set at the current shear force level when flexural yielding occurs. This procedure ensures that shear yielding coincides with flexural yielding, irrespective of the shear yield level originally specified.

The first approach has been adopted in modelling beam and wall members of coupled wall systems. The second approach has been used for the analysis of isolated walls in this investigation. These two approaches are based on the concept that shear yielding coincides with flexural yielding.

Interaction Between Moment and Axial Force. Inelastic behavior of a member subjected to moments and axial forces that change in the process of loading is discussed here.

A series of idealized moment-curvature relationships for different values of constant axial force is shown in Fig. A5. During loading the axial force on a section is subject to

change. The moment-curvature curve of a section under changing axial load is traced by appropriate shifts between the series of moment-curvature curves for constant axial loads as shown by the dashed lines in Fig. A5. It is assumed that the axial force is small enough that the axial force-moment interaction curve is in the linear range between the net tension strength and the balanced point as illustrated in Fig. A9. Cases where the axial compressive forces are above the balanced point are not considered.

Axial rigidity is affected by cracking depth and inelasticity in the reinforcement and concrete. In order to simplify the problem, it is assumed that the axial rigidity is related only to the curvature and axial strain of the section. Therefore, the flexural and axial actions of a section are correlated to each other. A procedure to calculate the instantaneous inelastic flexural and axial rigidities of a section, taking into account the effect of axial force on the moment-curvature curve and the effect of curvature on the axial force-axial strain curve is briefly explained here. The details of the procedure are described in Ref. 8.

It is assumed that the moment is a function of curvature and axial force, and the axial force is a function of curvature and axial strain. Therefore, the moment and the axial force are expressed in the following forms, respectively.

$$m = M(\Phi, n)$$

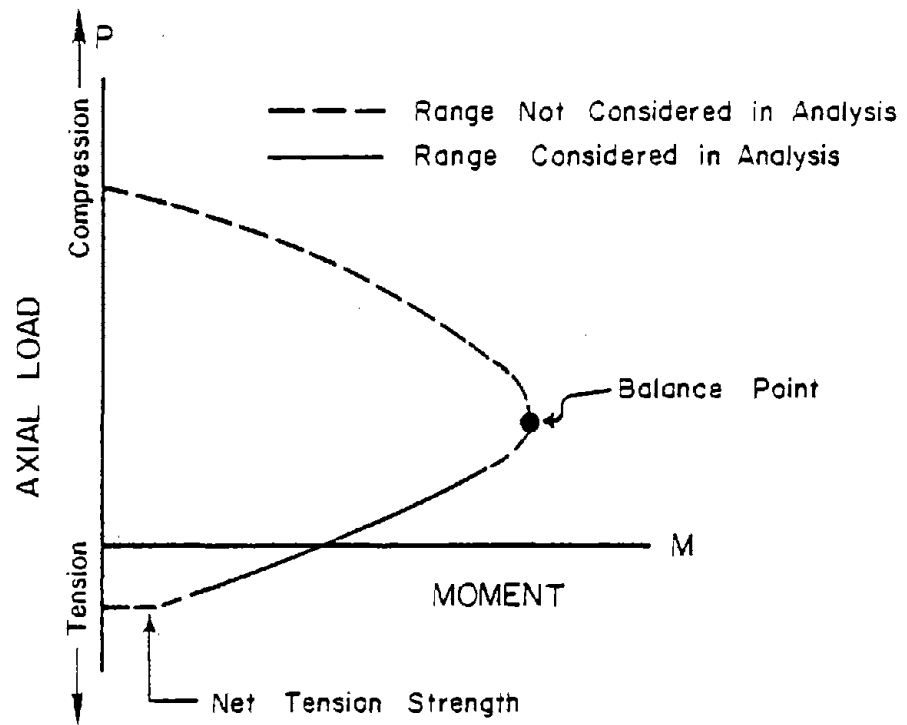$$n = N(\Phi, \varepsilon)$$

(A14)

where

Fig. A9   Axial-Force-Versus-Moment Interaction Diagram

m = bending moment at a section

n = axial force at a section

M = bending moment function

N = axial force function

Φ = curvature

ε = axial strain

The incremental forms of moment, m, and axial force, n, can be expressed by partially differentiating Eq. A14 with respect to each parameter.

$$\Delta m = \frac{\partial M}{\partial \Phi} \quad + \frac{\partial M}{\partial n} \Delta n \tag{A15}$$

$$\Delta n = \frac{\partial N}{\partial \Phi} \Delta \Phi + \frac{\partial N}{\partial \varepsilon} \Delta \varepsilon \tag{A16}$$

where

Δm = increment of moment

Δn = increment of axial force

ΔΦ = increment of curvature

Δε = increment of axial strain

After substituting Eq. A16 for n in Eq. A15, the following equations can be derived in matrix form.

$$\begin{Bmatrix} \Delta m \\ \Delta n \end{Bmatrix} = \begin{bmatrix} \frac{\partial M}{\partial \Phi} + \frac{\partial M}{\partial n}\frac{\partial N}{\partial \Phi} & \frac{\partial M}{\partial n}\frac{\partial N}{\partial \varepsilon} \\ \frac{\partial N}{\partial \Phi} & \frac{\partial N}{\partial \varepsilon} \end{bmatrix} \begin{Bmatrix} \Delta \Phi \\ \Delta \varepsilon \end{Bmatrix} \tag{A(17)}$$

This stiffness matrix is not symmetric because of the assumption made in Eq. A14. In order to restore symmetry in the stiffness matrix, Eq. A17 is rewritten by taking an inverse of Eq. A17. Then the inverse is used to express $\frac{\Delta m}{\Delta \Phi}$ in terms of $\frac{\partial M}{\partial \Phi}$ and a modification factor, and $\frac{\Delta n}{\Delta \varepsilon}$ in terms of $\frac{\partial N}{\partial \varepsilon}$ and a modi-

fication factor as follows:

$$
\left\{ \begin{array}{c} \Delta m \\ \\ \Delta n \end{array} \right\} = \left[\begin{array}{cc} \dfrac{\partial M}{\partial \Phi} \left(\dfrac{1}{1 - \dfrac{\partial M}{\partial n} \dfrac{\Delta n}{\Delta m}} \right) & 0 \\ & \\ 0 & \dfrac{\partial N}{\partial \varepsilon} \left(\dfrac{1}{1 - \left(\dfrac{\partial N}{\partial \Phi} \quad \dfrac{\partial M}{\partial \Phi} \right) \left(\dfrac{\Delta m}{\Delta n} - \dfrac{\partial M}{\partial n} \right)} \right) \end{array} \right] \left\{ \begin{array}{c} \Delta \Phi \\ \\ \Delta \varepsilon \end{array} \right\}
\tag{A18}
$$

It is assumed that the ratio of the increment of axial force over that of moment, $\dfrac{\Delta n}{\Delta m}$, does not change markedly during the loading process. Therefore, the previous step value of $\dfrac{\Delta n}{\Delta m}$ is used for the matrix terms in Eq. A18 to avoid an iterative process.

The value of $\dfrac{\partial M}{\partial \Phi}$ can be derived from the idealized moment-versus-curvature hysteresis loop for the corresponding axial force acting on the section. The value of $\dfrac{\partial N}{\partial \varepsilon}$ can be calculated by referring to the idealized axial force-axial strain curve for a given curvature.

Two diagonal terms in the matrix of Eq. A18 are considered as the current effective flexural rigidity and the current effective axial rigidity, respectively. On the other hand, $\dfrac{\partial M}{\partial \Phi}$ and $\dfrac{\partial N}{\partial \varepsilon}$ can be considered as pseudo-rigidities.

The current effective flexural rigidity represents the slope of the moment-curvature curve, including the effect of a changing axial force. The current effective axial rigidity represents the slope of the axial force-axial strain curve including the effect of a changing curvature. The pseudo-flexural rigidity is the slope of the moment-curvature curve with constant axial force acting on the section. The pseudo-axial rigidity is the slope of the axial force-axial strain curve for constant curvature.

Deformational Properties of Members

Deformational properties of members can be determined by integrating sectional properties over the member length. Since beams and walls are modelled in different forms, developments of the deformational property models for beams and walls are discussed separately.

Beam Deformational Properties. A beam member has shear force and bending moment as its force components, and lateral displacement and rotation as its displacement components. These components are specified at the member ends.

Rotational springs are placed at the ends of each connecting beam to consider the rotation due to inelastic flexural action over the beam length, strain in embedded tensile reinforcement at the ends of the beam, and shear deformation within the span of the beam. The linear flexible beam element spans between the rotational springs. The definition of moments and rotations at beam ends is illustrated in Fig. A10.

A) Rotation due to Inelastic Flexural Action. Inelastic flexural action in the connecting beam is assumed to be localized at the ends of the beam since the beam is exposed to antisymmetric distribution of moment along its length. There is a natural correspondence between the deformational properties of the rotational springs and the fixed-end-moment-versus-free-end-displacement relationship of a cantilever beam.

End rotations of a simply supported member subjected to an antisymmetric moment distribution can be related to the defor-
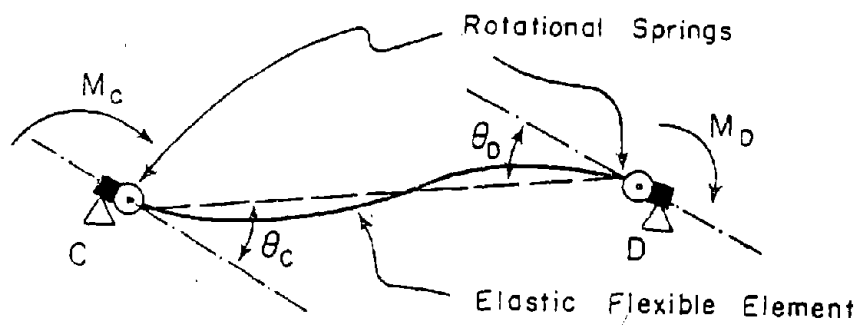
Fig. A10   Moment and Rotation at Beam Ends

mations of two cantilevers as discussed by Otani[10]. There-
fore, the deformational properties of the rotational springs in
the inelastic region can be derived by calculating the moment-
displacement curve of a cantilever whose span is half the clear
span length of the connecting beam. This assumes that the point
of contraflexure is fixed at midspan of the connecting beam. To
make the procedure applicable to beams of arbitrary length, a
cantilever with unit length is considered in the analysis.

For a cantilever, the curvature distribution can be defined
for a given fixed end moment using Eq. A8. Displacement at the
free end of the cantilever beam is then calculated from the
curvature distribution by computing the first moment of the
curvature diagram about the free end.

The free end displacement, (M), of the cantilever with unit
length can be expressed as a function of the fixed end moment,
M, by the following equations:

$$\delta(M) = \frac{M}{3EI_1} \qquad\qquad\qquad\qquad\qquad\qquad M \leq M_c$$

$$\delta(M) = \frac{M}{3}\left\{\frac{1}{EI_2} + \alpha^3\left(\frac{1}{EI_1} - \frac{1}{EI_2}\right)\right\} \qquad M_c \leq M \leq M_y \qquad (A19)$$

$$\delta(M) = \frac{M}{3}\left\{\frac{1}{EI_3} + \alpha^3\left(\frac{1}{EI_1} - \frac{1}{EI_2}\right) + \beta^3\left(\frac{1}{EI_2} - \frac{1}{EI_3}\right)\right\}$$

$$M_y \leq M$$

where

$$\alpha = \frac{M_c}{M}$$

$$\beta = \frac{M_y}{M}$$

With the moment-versus-displacement relationship of a unit length cantilever available, the relationship for a cantilever beam of any length can be derived by simply multiplying the relationship for a unit length cantilever by the square of the length for the desired span.

The idealized moment-displacement relationship of a unit length cantilever is established by trilinearizing the original curve expressed by Eq. A19. The origin, cracking, yielding and ultimate points on the curve are connected successively by straight lines. The ultimate moment is defined as the point where the extreme compressive fiber strain reaches 0.004.

Slopes in the three stages of the idealized moment-versus-displacement relationship are defined as follows:

$$S(M) = \frac{M_c}{\delta_c} \qquad\qquad M \leq M_c$$

$$S(M) = \frac{M_y - M_c}{\delta_y - \delta_c} \qquad\qquad M_c \leq M \leq M_y \qquad\qquad (A20)$$

$$S(M) = \frac{M_u - M_y}{\delta_u - \delta_y} \qquad\qquad M_y \leq M$$

where

$S(M)$ = instantaneous stiffness of unit length cantilever

δ_c = cracking displacement of unit length cantilever

δ_y = yielding displacement of unit length cantilever

δ_u = ultimate displacement of unit length cantilever

The incremental rotation of the rotational spring due to inelastic flexural action can be expressed approximately by the instantaneous stiffness, $S(M)$, since inelastic flexural action is assumed to be localized at the beam end. Accordingly,

$$\Delta\theta = \frac{L}{2S(M)} \Delta M \tag{A21}$$

where

$\Delta\theta$ = incremental rotation

ΔM = incremental moment

L = length of beam

Equation A21 is used as a part of the instantaneous moment-versus-rotation relationship of the rotational springs in the analysis.

B) <u>Rotation Due to Inelastic Shear Deformation</u>. In addition to the flexural deformation of the connecting beams, rotation due to shear deformation of the beams is also taken into account in this investigation.

It is assumed that the inelastic shear rigidity reduces in direct proportion to the inelastic flexural rigidity. Therefore, the ratio of the incremental displacement based solely on flexural rigidity to that based on both flexural and shear rigidities is considered to remain constant during any stage of inelastic action.

This displacement ratio is considered as a modifying factor to be applied to the instantaneous flexural stiffness, S(M). The displacement ratio can be expressed as follows:

$$\frac{\Delta\delta_f}{\Delta\delta} = \frac{1}{\dfrac{3EI_i}{GA_i L^2} + 1} \tag{A22}$$

where

$\Delta\delta_f$ = incremental displacement due to flexural rigidity only

$\Delta\delta$ = increment of the total free end displacement

EI_i = instantaneous flexural rigidity

GA_i = instantaneous shear rigidity

Thus the stiffness which includes the shear deformation effect can be expressed as

$$ST(M) = S(M) \frac{\Delta\delta_f}{\Delta\delta} \qquad (A23)$$

where

$S(M)$ = instantaneous stiffness based on flexural rigidity

$ST(M)$ = instantaneous stiffness based on flexural and shear rigidity

For the case where rotation due to shear deformation is considered in the analyses, the instantaneous stiffness $ST(M)$ is used instead of $S(M)$ in Eq. A21.

C) Rotation due to Strain of Tensile Reinforcement Embedded in the Wall. Rotation due to strain of tensile reinforcement along its embedded length in the wall is considered as an additional flexibility factor for the rotational spring at the and of a beam.

Bond stress is assumed to be constant along the embedded length of the renforcement. Therefore, the tensile stress in the reinforcement decreases linearly with distance from the face of the wall.

It is assumed that the reinforcement embedment length is sufficient to sustain the maximum tensile stress occurring in the loading process. The strain hardening portion of the stress-strain curve for the reinforcement is idealized as a straight line connecting the yield point and the point at maximum strength. Elongation of reinforcement over the development length is calculated by integrating the strain over the length.

If the stress in the reinforcement exceeds the yield stress, f_y, the development length is divided into two parts, as shown in Fig. A11. A drastic reduction in axial ridigity of the reinforcement takes place at yielding. Therefore, integration of strain must be performed separately over the two parts of the development length from the point of zero stress to that of the yield stress, and from the point of the yield stress to that of the maximum stress. Strain in compressive reinforcement embedded in the walls is assumed to by zero.

Based on the assumptions made here, the rotation versus moment relationship can be expressed as follows:

$$\omega = \frac{1}{8} \frac{D}{E_s u} \left(\frac{f_y}{M_y}\right)^2 M^2 \frac{1}{(d - d')} \qquad M \leq M_y \tag{A24}$$

$$\omega = \left[\frac{Df_y^2}{4u} \frac{1}{E_s} \left(\frac{M}{M_y} - \frac{1}{2}\right) + \frac{1}{2E_y}\left(\frac{M}{M_y} - 1\right)^2\right] \frac{1}{(d - d')}$$
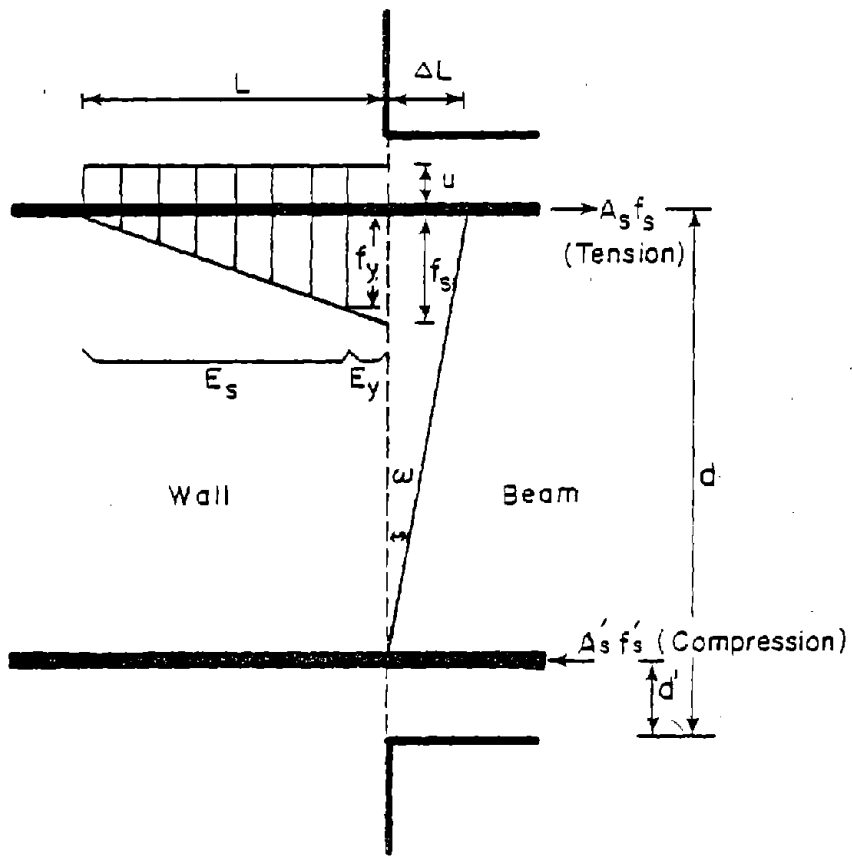$$M_y \leq M$$

Fig. A11   Distribution of Stress in Tensile
Reinforcement Embedded in the Wall

where

ω = rotation due to strain in embedded tensile reinforcement

M = bending moment at the beam end

M_y = yielding moment at the beam end

D = diameter of a reinforcing bar

u = average bond stress

E_s = Young's modulus of the reinforcement

E_y = inelastic modulus of the reinforcement after yielding

f_y = yielding stress of the reinforcement

d = depth of the tensile reinforcement

d' = depth of the compressive reinforcement

Details of the derivation of Eq. A24 are described in Ref. 8.

The idealized form of the moment-rotation relationship is again obtained by trilinearizing the original curve, successively connecting points at the origin, cracking, yielding and ultimate moments.

The flexibilities in the three stages of the idealized moment-rotation relationship are defined as follows:

$$f(M) = \frac{\omega_c}{M_c} \qquad\qquad M \leq M_c$$

$$f(M) = \frac{\omega_y - \omega_c}{M_y - M_c} \qquad\qquad M_c \leq M \leq M_y \qquad (A25)$$

$$f(M) = \frac{\omega_u - \omega_y}{M_u - M_y} \qquad\qquad M_y \leq M$$

where

$f(M)$ = flexibility resulting from the bond slippage of tensile reinforcement of a beam

ω_c = rotation corresponding to the cracking moment, calculated from Eq. A24

ω_y = rotation corresponding to the yielding moment, calculated from Eq. A24

ω_u = rotation corresponding to the ultimate moment, calculated from Eq. A24

The incremental rotation of the rotational spring due to strain in embedded reinforcement can be expressed by the flexibility, $f(M)$, as follows:

$$\Delta\theta = f(M)\,\Delta M \tag{A26}$$

Equation A26 is used as a part of the instantaneous moment-rotation relationship of a rotational spring in the analysis.

Moments and rotations at beam ends are related through a flexibility matrix that can be established as the sum of several types of flexibility as discussed in preceding paragraphs. The flexibility matrix, excluding the vertical displacement components, can be calculated by simply adding the flexibilities of the rotational springs to those due to elastic flexural actions in the flexible element. The flexibility matrix is expressed as:

$$\begin{bmatrix} f_{CC} & f_{CD} \\ f_{DC} & f_{DD} \end{bmatrix} = \begin{bmatrix} \dfrac{L}{6EI} & -\dfrac{L}{6EI} \\ -\dfrac{L}{6EI} & \dfrac{L}{6EI} \end{bmatrix} + \begin{bmatrix} \dfrac{L}{2ST(M_C)} + f(M_C) & 0 \\ 0 & \dfrac{L}{2ST(M_D)} + f(M_D) \end{bmatrix} \qquad (A27)$$

where

L = length of the beam clear span

EI = elastic flexural rigidity of the flexible element

$\dfrac{L}{2ST(M_C)}$ and $\dfrac{L}{2ST(M_D)}$ = rotational flexibilities due to the inelastic flexural and shear actions over the beam length, defined in Eq. A23

$f(M_C)$ and $f(M_C)$ = rotational flexibilities due to the reinforcement strain in the joint core, defined in Eq. A26

M_C and M_D = moments at the clear span ends of the beam

In the development of Eq. A27, part of the elastic flexibility coefficients of the diagonal elements in the first matrix on the right-hand side of the equation have been assigned to the term, $L/2ST(M)$, in the second matrix. In the second matrix, the flexibility constants, $L/2ST(M)$ and $f(M)$, are functions of the existing moment level and the loading history of the rotational spring.

It should be noted that the off-diagonal terms reflecting the interaction between opposite end rotations depend solely on the elastic flexible terms.

A-38

Incremental end rotations of the combined rotational spring-
flexible element system are related to incremental end moments
through the combined flexibility matrix as

$$\left\{ \begin{array}{c} \Delta\theta_C \\ \Delta\theta_D \end{array} \right\} = \left[\begin{array}{cc} f_{CC} & f_{CD} \\ f_{DC} & f_{DD} \end{array} \right] \left\{ \begin{array}{c} M_C \\ M_D \end{array} \right\} \tag{A28}$$

where

$\Delta\theta_C$ and $\Delta\theta_D$ = incremental rotations at the
clear span ends of the beam

ΔM_C and ΔM_D = incremental moments at the clear span
ends of the beam

Wall Deformational Properties. A wall member has axial
force, shear force and bending moment as its force components,
and axial displacement, lateral displacement and rotation as its
displacement components. These member force and displacement
components are shown in Fig. A12.

Each wall member is considered to consist of several sub-
elements so that each subelement can be subjected to a different
stage of inelastic action. The stiffness properties of each
subelement are assumed to be constant over the length of the
subelement.

For the time being, the wall member is considered as a
cantilever to facilitate calculations of the member deforma-
tional properties. The member deformational properties are
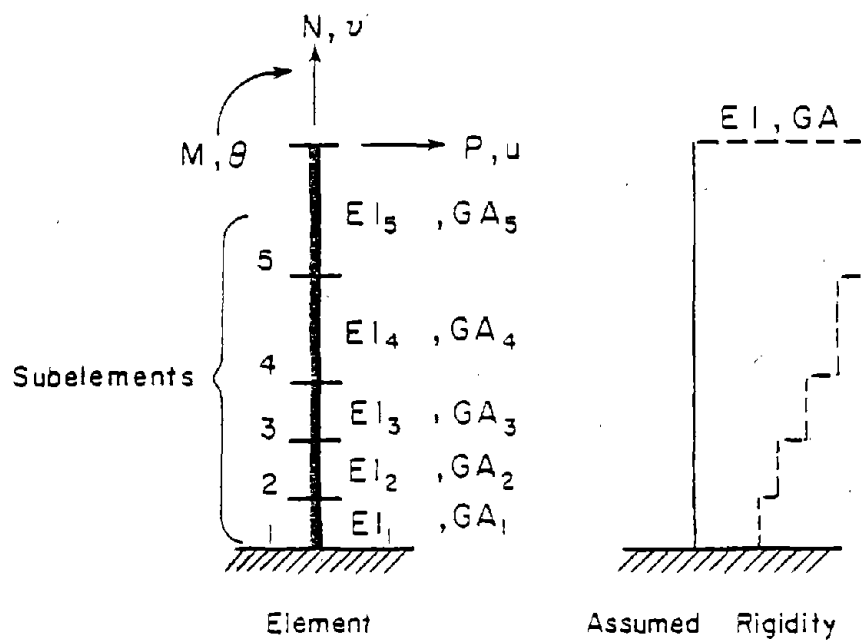calculated from the section properties of each subelement. The

Fig. A12   Divided Element Model for Walls

configuration of the cantilever is shown in Fig. A12. The flexibility matrix of the cantilever can be derived by using the transformation matrix and the flexibility matrix of each element as follows:

$$f_c = \sum_{j=1}^{n} \left[T_j \right]^T \left[f_j \right] \left[T_j \right] \tag{A29}$$

where

$\left[f_c \right]$ = flexibility matrix of the cantilever

$\left[f_j \right]$ = flexibility matrix of the j th subelement

$\left[T_j \right]$ = transformation matrix of the j th subelement with respect to the free end

$\left[T_j \right]^T$ = transpose matrix of T_j

n = the number of subelements in the member.

The matrices used in Eq. A29 can be expressed as follows:

$$\left[f_j \right] = \begin{bmatrix} \dfrac{\ell_j}{EA_{ij}} & 0 & 0 \\[2ex] 0 & \dfrac{\ell_j^3}{3EI_{ij}} + \dfrac{\ell_j}{GA_{ij}} & -\dfrac{\ell_j^2}{2EI_{ij}} \\[2ex] 0 & -\dfrac{\ell_j^2}{2EI_{ij}} & \dfrac{\ell_j}{EI_{ij}} \end{bmatrix} \tag{A30}$$

$$\left[T_j \right] = \begin{bmatrix} 1 & 0 & 0 \\[1ex] 0 & 1 & 0 \\[1ex] 0 & -L + \displaystyle\sum_{n=1}^{j} \ell_j & 1 \end{bmatrix} \tag{A31}$$

where

$$L = \text{total length of the cantilever}$$

$$\ell_j = \text{length of the } j \text{ th subelement}$$

$$EA_{ij} = \text{instantaneous axial rigidity of the } j \text{ th subelement}$$

$$GA_{ij} = \text{instantaneous shear rigidity of the } j \text{ th subelement}$$

$$EI_{ij} = \text{instantaneous flexural rigidity of the } j \text{ th subelement}$$

These subelement rigidities can be calculated from Eqs. A13 and A18. Equation A29 is considered to be the basic formulation to express the deformational properties of walls. The stiffness matrix of wall members can be developed based on Eq. A29 as discussed in Appendix B.

Hysteresis Rules

A hysteretic moment-rotation relationship following the rules proposed by Takeda et al[11] has been adopted for the instantaneous flexural stiffness terms in this investigation. The basic shear-force-versus-shear-distortion relationship for the inelastic shear stiffness is also assumed to follow Takeda's hysteresis loop.

The primary curve of the hysteresis loop is established by connecting the origin, cracking point, yielding point and ulti-mate point successively by straight lines, thus forming the tri-linearized curve. No limit on the third slope is considered

for the primary curve. The loading curve is basically directed toward the previous maximum point on the primary curve in that direction. The slope of the unloading curve is degraded depending on the maximum deflection reached in either direction.

Details of Takeda's hysteresis rules are given in Ref. 10. These rules have to be modified to deal with some specific features that appear in the behavior of constituent members of the coupled wall systems under lateral loads.

Interaction Among Axial, Flexural and Shear Components. For the wall subelements the moment-curvature curves for different values of axial force are trilinearized as shown in Fig. A5. Cracking and yielding levels are shifted in accordance with the value of axial force.

The current moment-curvature curve is chosen to be the one corresponding to the current level of axial force. The pseudo-rigidity, $\frac{\partial M}{\partial \Phi}$ in Eq. A18, obtained from the slope of the current moment-curvature curve, follows Takeda's hysteresis rules. The real flexural rigidity can be obtained by multiplying $\frac{\partial M}{\partial \Phi}$ by a factor reflecting the effect of transferring from one moment-curvature curve to another due to the change of axial force. This factor is defined in Eq. A18. An actual hysteresis loop for a wall subelement is given by the thick solid curves in Fig. A13. The detailed procedure for evaluating $\frac{\partial M}{\partial \Phi}$ and $\frac{\partial M}{\partial n}$ was discussed in Ref. 8.
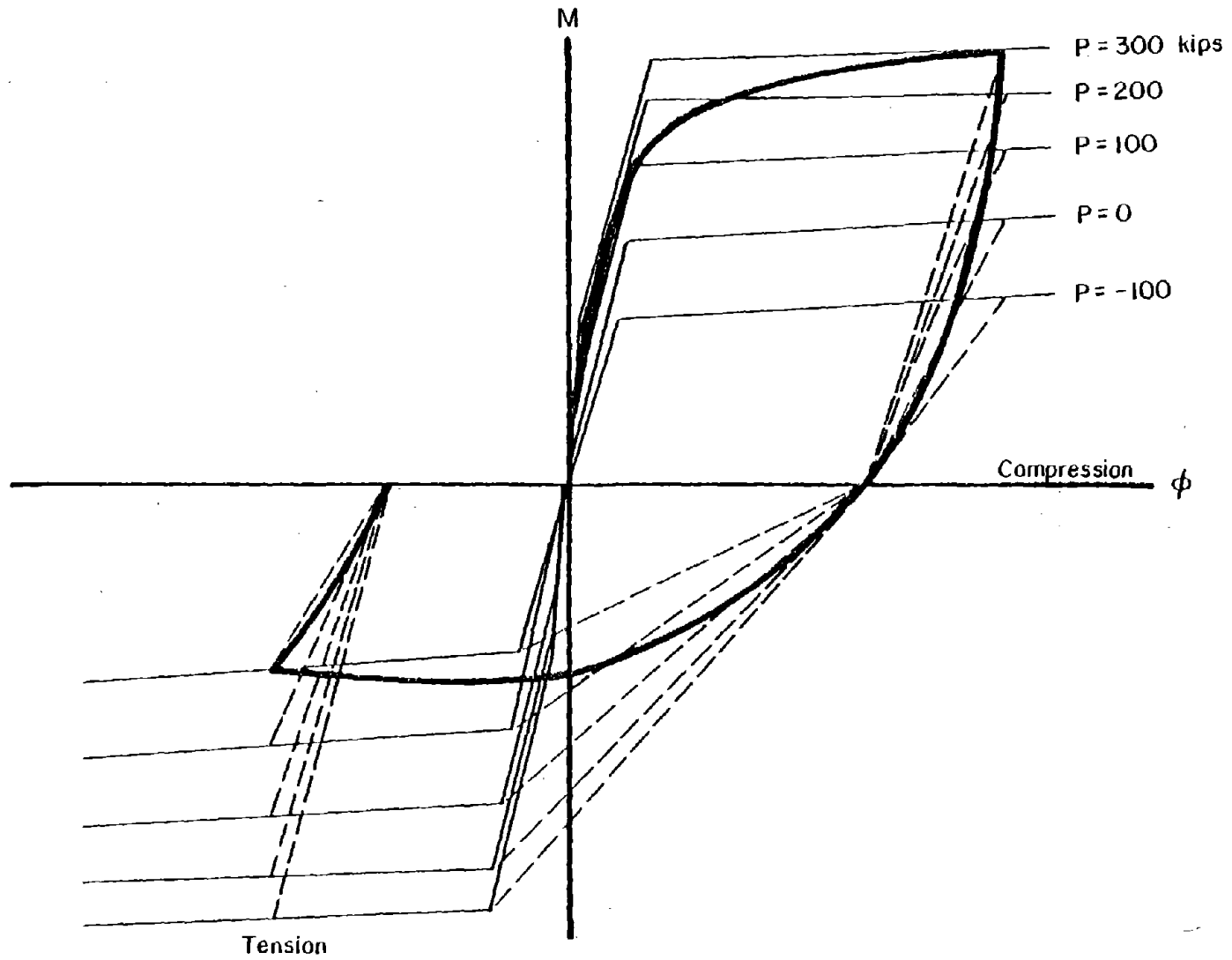
Fig. Al3   Hysteresis Loop with Effect of Changing Axial Force

The curves of the axial force-axial strain relationships for different values of curvature are idealized by a set of straight lines with two boundary lines as shown in Fig. A7. The working axial force-axial strain curve is assumed to be the one corresponding to the current value of curvature. The pseudo-axial rigidity, $\frac{\partial N}{\partial \varepsilon}$ in Eq. A18, is considered as the slope of the the current axial force-axial strain curve.

Because of lack of data for this relationship, no hysteretic properties are given to the axial force-axial strain curves in this analysis. Therefore, its unloading curve follows the same trace as the loading curve. In other words, the axial force, axial strain, and curvature can be related to one another irrespective of the previous loading history.

In addition to the interaction between axial and flexural components mentioned above, coupling between shear yielding and flexural yielding has been introduced in an approximate way. Shear yielding occurs whenever flexural yielding occurs, independent of the shear yield level originally specified.

Pinching Action and Gradual Strength Loss of Shear Hysteresis Properties. Modifications to the conventional type of hysteresis model have been introduced to permit more realistic modeling of the shear-force-versus-shear-distortion relationship.

Two significant features have been incorporated in the shear hysteresis properties. One is a gradual loss of strength with repeated load reversals beyond a specified shear deformation, and the other is pinching action in the reloading branch.

The strength softening is primarily due to the distorted concrete section and the permanent strain accumulated in the shear reinforcement. These are related to the number of reversals and the previous maximum shear distortion.

After the working hysteresis loop has exceeded the strength, a strength loss is introduced in the hysteresis loop on subsequent cycles. The rate of strength loss is assumed to increase proportionally with deformation.

A guideline is introduced in the hysteresis loop to include the effect of strength loss in the analysis as shown in Fig. A14. The reloading branch does not go to the previous maximum deformation. Instead, it is directed towards a point corresponding to the previous maximum distortion. Beyond this point the hystersis loop runs parallel to the third slope of the original primary curve.

Pinching action is attributed mainly to the fact that before previously formed cracks in the compressive zone concrete can close, dowel action of the reinforcement across the cracks provides the sole resistance to the applied shear force. The "pinching" action is observed in hysteresis loops obtained from tests on wall specimens.

This feature is considered in the analysis by introducing a
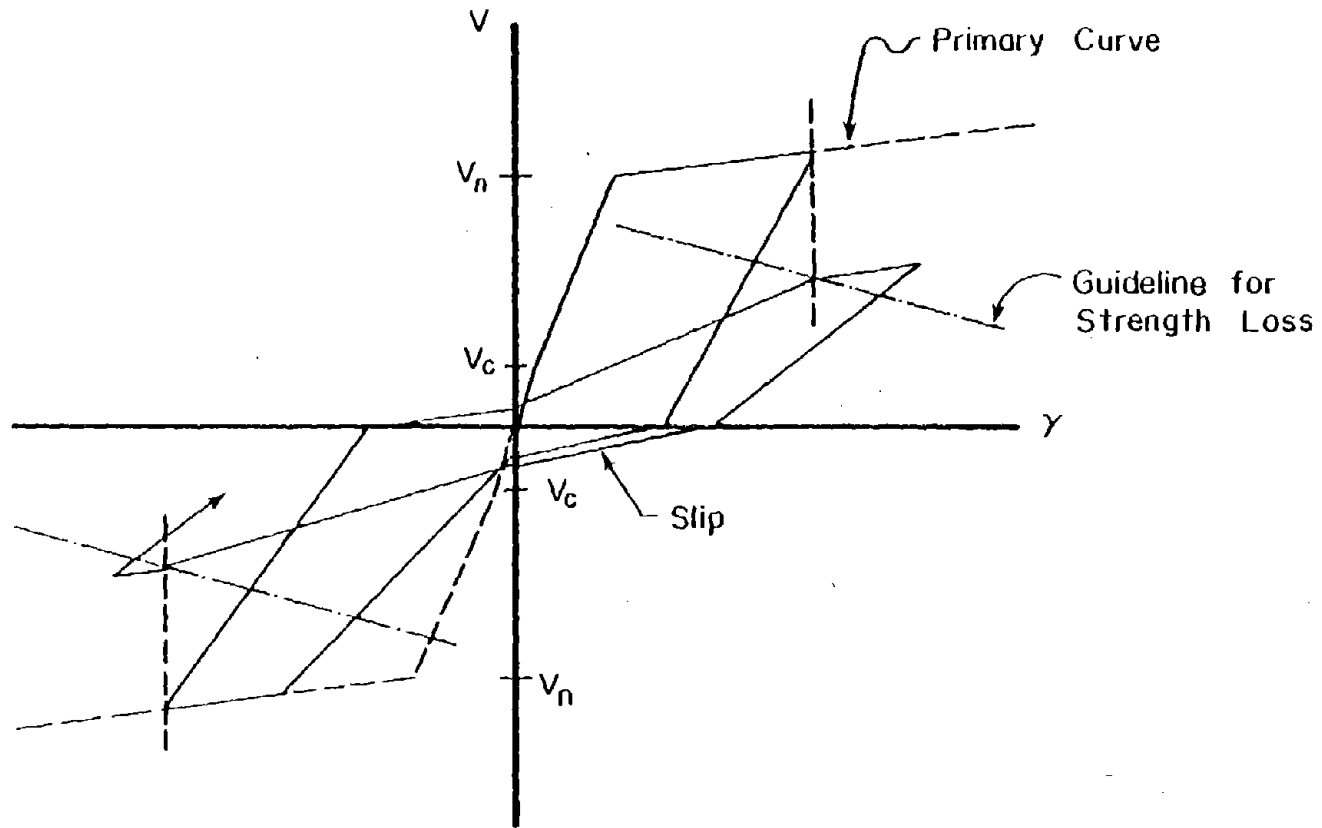
Fig. A14   Hysteresis Loops with Effects of Slip Action
and Strength Loss

reduced shear stiffness in place of the current reloading slope whenever a branch of the hysteresis loop is located in the second or fourth quadrant as shown in Fig. A14.

The options of strength loss and pinching action are considered for the shear-versus-shear-distortion relationship of isolated wall members in this analysis. The same options are also used for the rotational springs of connecting beam members, because no separate inelastic shear spring is provided for the connecting beams.

APPENDIX B - ASSEMBLAGE OF STRUCTURAL STIFFNESS MATRIX

AND CALCULATION OF FAILURE MECHANISM FORMATION

The procedures for assemblying the structural stiffness matrix and tracing the failure mechanism formation are discussed in this Appendix.

Member Stiffness Matrix

A computational procedure to develop the stiffness matrix of each constituent member is described here. Member stiffness matrices are derived from the flexibility matrices developed in Appendix A.

Beam Member Stiffness Matrix. The beam is connected to each wall through a rigid link and a rotational spring as shown in Fig. B1. The rotational spring models the inelastic flexural and shear actions within the beam length as well as the beam end rotations due to bond slip in the joint core as described in the main body of the report.

The flexibility matrix for a simply supported connecting beam excluding the rigid links, is expressed by Eq. A27 in Appendix A. The stiffness matrix can be obtained by inverting the flexibility matrix. A transformation matrix relates the member end components of the elastic flexible beam to those of the total connecting beam system including the rigid links. The instantaneous moment-rotation relationship of a simply sup-

Fig. B1 Deformed Configuration of Connecting
Beam Systems

ported system that consists of the rigid links, rotational springs and flexible beam can be expressed as follows:

$$
\left\{ \begin{array}{c} \Delta M_A \\ \Delta M_B \end{array} \right\} = \begin{bmatrix} 1+\lambda & \lambda \\ \lambda & 1+\lambda \end{bmatrix} \begin{bmatrix} K_{CC} & K_{CD} \\ K_{DC} & K_{DD} \end{bmatrix} \begin{bmatrix} 1+\lambda & \lambda \\ \lambda & 1+\lambda \end{bmatrix} \left\{ \begin{array}{c} \Delta\theta'_A \\ \Delta\theta'_B \end{array} \right\}
\qquad (B1)
$$

where

λ = ratio of the length of a rigid link to that of a flexible beam

K_{CC}, K_{CD}, K_{DC} and K_{DD} = stiffness terms derived from the inverse of the flexibility matrix in Eq. A28 in Appendix A.

$\Delta\theta'_A$ and $\Delta\theta'_B$ = incremental rotations at the ends of a simply-supported beam system with the rigid links

ΔM_A and ΔM_B = incremental moments at the ends of a simply-supported beam system with the rigid links

Actual interpretation of $\Delta\theta'_A$ and $\Delta\theta'_B$ in a deformed configuration is shown in Fig. B1.

Neither shear forces nor lateral displacements at the member ends are considered in Eq. B1. In order to include these member end components missing in Eq. B1 in the final form, the incremental end rotations, $\Delta\theta'_A$ and $\Delta\theta'_B$, of a simply supported beam system should be expressed in terms of incremental end rotations, $\Delta\theta_A$ and $\Delta\theta_B$, measured from the horizontal position

and incremental end vertical displacements, Δv_A and Δv_B, that are related through a transformation matrix. These member end components are illustrated in Fig. B1.

Similarly, the incremental member end shear forces, ΔN_A and ΔN_B, can be related to the incremental member end moments, ΔM_A and ΔM_B, through a transposed form of the same transformation matrix.

The final force-displacement relation of a connecting beam system is expressed in the following form.

$$
\begin{Bmatrix} \Delta N_A \\ \Delta M_A \\ \Delta N_B \\ \Delta M_B \end{Bmatrix} = \begin{bmatrix} \frac{1}{L(1+2\lambda)} & \frac{1}{L(1+2\lambda)} \\ 1 & 0 \\ \frac{-1}{L(1+2\lambda)} & \frac{-1}{L(1+2\lambda)} \\ 0 & 1 \end{bmatrix} \begin{bmatrix} 1+\lambda & \lambda \\ \lambda & 1+\lambda \end{bmatrix} \begin{bmatrix} K_{CC} & K_{CD} \\ K_{DC} & K_{DD} \end{bmatrix}
$$

$$
\times \begin{bmatrix} 1+\lambda & \lambda \\ \lambda & 1+\lambda \end{bmatrix} \begin{bmatrix} \frac{1}{L(1+2\lambda)} & 1 & \frac{-1}{L(1+2\lambda)} & 0 \\ \frac{1}{L(1+2\lambda)} & 0 & \frac{-1}{L(1+2\lambda)} & 1 \end{bmatrix} \begin{Bmatrix} \Delta v_A \\ \Delta \theta_A \\ \Delta v_B \\ \Delta \theta_B \end{Bmatrix} \qquad (B2)
$$

where

ΔN_A and ΔN_B = incremental shear forces at the ends of a connecting beam system

Δv_A and Δv_B = incremental lateral displacements at the ends of a connecting beam system

$\Delta \theta_A$ and $\Delta \theta_B$ = incremental rotations at the ends of a connecting beam system measured from the horizontal position

With the global coordinate system also adopted as the local coordinate system for the connecting beam, these member end components are also considered as the beam contribution to the formulation of the structural stiffness matrix.

Wall Member Stiffness Matrix. Stiffness matrix of a cantilever beam can be obtained as the inverse of the flexibility matrix of the cantilever beam. The flexibility matrix of the cantilever beam is expressed by Eq. A29. The member stiffness matrix of a wall member can be developed on the basis of the stiffness matrix of the cantilever beam using conventional matrix formulation. The member stiffness matrix relates the incremental member end forces to the incremental member end displacements as follows:

$$
\left\{
\begin{array}{c}
\Delta N_A \\
\Delta P_A \\
\Delta M_A \\
\hline
\Delta N_B \\
\Delta P_B \\
\Delta M_B
\end{array}
\right\}
=
\left[
\begin{array}{c|c}
T_{AB} \, K_{AB} \, T_{AB}^T & - T_{AB} \, K_{AB} \\
\hline
- K_{AB} \, T_{AB}^T & K_{AB}
\end{array}
\right]
\left\{
\begin{array}{c}
\Delta v_A \\
\Delta u_A \\
\Delta \theta_A \\
\hline
\Delta v_B \\
\Delta u_B \\
\Delta \theta_B
\end{array}
\right\}
\quad (B3)
$$

where

$\left[K_{AB} \right]$ = three by three stiffness matrix of the cantilever beam (the inverse of f_c in Eq. A29 in Appendix A.

$\left[T_{AB} \right]$ = transformation matrix of the cantilever beam

$$
\left[T_{AB} \right] =
\begin{bmatrix}
1 & 0 & 0 \\
0 & 1 & 0 \\
0 & -L & 1
\end{bmatrix}
$$

$$\left[T_{AB} \right]^T = \text{transpose matrix of } \left[T_{AB} \right]$$

ΔN_A and ΔN_B = incremental axial forces at the ends of a wall member

ΔP_A and ΔP_B = incremental shear forces at the ends of a wall member

ΔM_A and ΔM_B = incremental moments at the ends of a wall member

Δv_A and Δv_B = incremental vertical displacements at the ends of a wall member

Δu_A and Δu_B = incremental lateral displacements at the ends of a wall member

$\Delta \theta_A$ and $\Delta \theta_B$ = incremental rotations at the ends of a wall member

These member end components can be considered as the joint displacements and forces, since the global coordinate system has also been adopted for the member coordinates. The member stiffness matrix contributes to the formulation of the total structural stiffness matrix.

Structural Stiffness Matrix

The instantaneous structural stiffness matrix is developed by superimposing at each joint stiffness contributions from all members connected at that joint. The internal degrees of freedom are condensed out of the structural stiffness matrix before the system equations are established so that only horizontal story movements appear in the final form of the equations. The incremental force-displacement relationship of a structure is expressed as follows:

$$
\left\{ \begin{array}{c} \Delta P \\ ---- \\ \Delta N \\ \Delta M \end{array} \right\} = \left[\begin{array}{c|c} K_{11} & K_{12} \\ \hline K_{21} & K_{22} \end{array} \right] \left\{ \begin{array}{c} \Delta u \\ ---- \\ \Delta v \\ \Delta \theta \end{array} \right\} \tag{B4}
$$

where

K_{11} = submatrix of size, I by I

K_{12} = submatrix of size, I by 2J

K_{21} = submatrix of size, 2J by I

K_{22} = submatrix of size, 2J by 2J

I = number of stories

J = number of joints

ΔP = incremental story lateral force vector

ΔN = incremental joint vertical force vector

ΔM = incremental joint moment vector

Δu = incremental story lateral displacement vector

Δv = incremental joint vertical displacement vector

$\Delta \theta$ = incremental joint rotation vector

Only external lateral loads are considered in the analysis. Static condensation of the vertical displacements and rotations results in an instantaneous structural stiffness matrix that relates the incremental lateral displacements to the incremental lateral forces as follows:

$$
\left\{ \Delta P \right\} = \left[\left[K_{11} \right] - \left[K_{12} \right] \left[K_{22} \right]^{-1} \left[K_{21} \right] \right] \left\{ \Delta u \right\} \tag{B5}
$$

With a given set of incremental lateral loads and a known

instantaneous structural stiffness, Eq. B5 can be solved for incremental lateral displacements.

Analysis for Static Loads

Static lateral loads applied to the structure can be either monotonically increasing loads or slowly reversed loads. A given set of lateral loads is applied to each story level of the structure in small increments. The load increments are chosen to be small enough to avoid any significant calculation error due to overshooting in the hystersis loop.

Equation B5 of the incremental lateral force-versus-displacement relationships is solved for the incremental lateral story displacements under a given set of lateral loads by a step-by-step procedure. The structural stiffness is assumed to be constant during a load increment. Incremental joint displacements and member forces are calculated at the end of each load increment.

Incremental vertical displacements and rotations at the joints are calculated from the following equation.

$$\begin{Bmatrix} \Delta v \\ \Delta \theta \end{Bmatrix} = -\begin{bmatrix} K_{22} \end{bmatrix}^{-1} \begin{bmatrix} K_{21} \end{bmatrix} \begin{Bmatrix} \Delta u \end{Bmatrix} \tag{B6}$$

Equation B6 can be derived in the process of the static condensation. Incremental member end forces are computed from the incremental member-end-forces-versus-displacement relationships

that are subject to the hysteresis rules. If a member force exceeds its specifed value, the member stiffness is modified at the beginning of the next load increment in accordance with the hysteresis rules. Finally, the current member end displacements and forces are evaluated by adding the computed incremental values to the accumulated values from the previous steps.

Formation of failure mechanisms in the structure and the failure process of each constituent member can be traced in the static analysis described above.

APPENDIX C- STATIC ANALYSIS OF ISOLATED STRUCTURAL WALLS

Isolated Structural Wall Tests

The analytical models were used to simulate slowly reversed loading tests of isolated walls conducted at the Construction Technology Laboratories.[7] Agreement between analytical and experimental results provides some justification for the use of the analytical models in the analysis of coupled wall systems.

Laboratory tests have been conducted on large-scale reinforced concrete isolated structural walls under monotonically increasing as well as slowly reversed loadings. The results of these tests indicate a strong relationship between flexural yielding and shear yielding. This was shown in the almost-simultaneous occurrence of shear yielding with flexural yielding. Further details of the experimental program are found in Ref. 7.

To check the reliability of the analytical model used in the analysis of coupled wall systems, results obtained using the analytical model were compared with experimental results for two selected isolated wall specimens. These specimens are denoted by B4 and B5 in Ref. 7.

Overall dimensions of Specimens B4 and B5 are given in Fig. C1. The test specimens are approximately one-third scale representations of full-size walls. Amounts of reinforcement used for different sections of the specimens are summarized in Table C1. Design yield stress of the reinforcement was 60 ksi (414 MPa) and design concrete strength was 6000 psi (41.4 MPa).
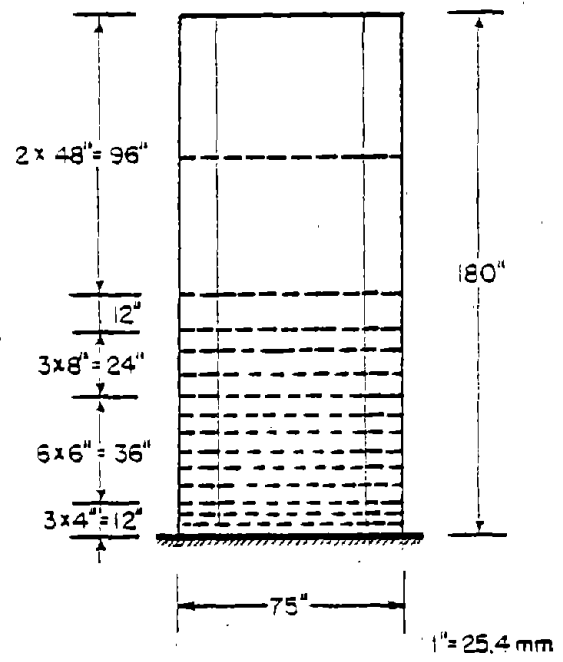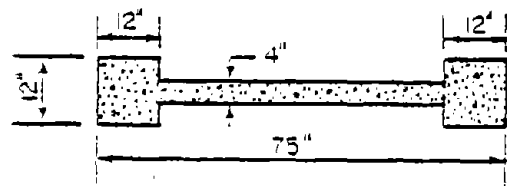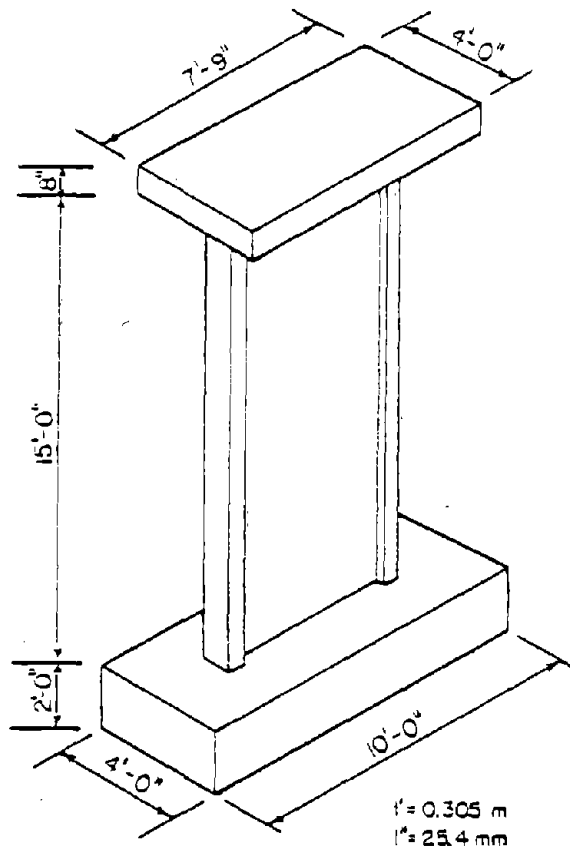
Fig. C1   Nominal Dimensions
          of Test Specimen

Fig. C2   Segmentation of Wall

TABLE C1 – REINFORCEMENT OF TEST SPECIMENS

Specimen	Reinforcement (%)			
	f	h	n	s
B4	1.11	0.31	0.29	1.28
B5	3.67	0.63	0.29	1.35

f = ratio of main flexural reinforcement area to gross concrete area of boundary element

h = ratio of horizontal shear reinforcement area to gross concrete area of a vertical section of wall web

n = ratio of vertical web reinforcement area to gross concrete area of a horizontal section of wall web

s = ratio of effective volume of confinement reinforcement to the volume of core in accordance with Eq. A.4 of ACI 318-71.

TABLE C2 – PRIMARY CURVES FOR SPECIMENS

	B4	B5
Flexural Properties		
Cracking Moment (kip-in.)	4,500	4,500
Yielding Moment (kip-in.)	9,000	24,000
First Rigidity (kip-in.^{2})	1,450,000,000	1,630,000,000
Second Rigidity (kip-in.^{2})	76,000,000	450,000,000
Third Rigidity (kip-in.^{2})	4,000,000	15,000,000
Shear Properties		
Cracking Shear (kip)	25	25
Yielding Shear (kip)	82	127
Shear Strength (kip)	106	107
First Rigidity (kip)	430,000	430,000
Second Rigidity (kip)	17,000	40,000
Third Rigidity (kip)	1,300	8,000
Slip Rigidity (kip)		4,000

1 kip = 4.4482 kN
1 kip-in. = 0.1130 kN-m
1 kip-in.^{2} = 0.00287 kN-m^2

The specimens were constructed with confinement reinforce-
ment in the lower 6 ft (1.83 m) of the boundary elements. Each
specimen was loaded as a vertical cantilever with a concentrated
horizontal load at the top. The load was monotonically
increased for B4 and cyclically reversed for B5. No axial force
was applied to either wall.

Analytical Procedure

The program SIVA2 was used to simulate the test of the two
isolated structural walls. Takeda's hysteresis rules are used
for the inelastic shear-force-versus-shear-distortion relation-
ship. Also considered in the program are strength loss, "pinch-
ing" effect, and coupling between shear and flexural yielding.

The primary curves for the moment-versus-curvature rela-
tionship and the shear-versus-shear-distortion relationship can
be determined by the procedure described in this report. The
slope of the reloading branch of the shear-force-versus-shear-
distortion relationship representing pinching can be based on
available test data. The rate of strength loss may also be
evaluated from experimental results. However, strength loss was
not considered in the analysis, since it is assumed that the
response will not exceed the deformation at which strength loss
occurs.

The parameters defining the primary curves used in the
analyses are summarized in Table C2. An idealized model of the
specimens is shown in Fig. C2. The wall is finely segmented in

the hinging region to take account of rapid changes in the inelastic behavior of this region. The load increment applied in each step is 1/150 of the maximum static load.

Comparison of Analytical and Experimental Results

The calculated results for Specimens B4 and B5 are compared with the measured results. Specimen B4 was subjected to a monotonically increasing load while Specimen B5 was tested under reversed cyclic loading. For specimen B5, the first two major cycles are simulated by limiting displacements in accordance with recorded data.

Three different assumptions were investigated for each of the two specimens.

Case 1 - The shear-versus-shear-distortion relationship is assumed to be linearly elastic, with all inelastic action in the wall being accounted for by flexural yielding.

Case 2 - Inelastic shear deformations are allowed in addition to flexural yield. No coupling is assumed between these two yielding mechanisms. The shear strength level is determined independently of flexure yielding.

Case 3 - Coupling between shear and flexural deformations is considered such that shear yielding is initiated whenever flexural yielding occurs.

Specimen B4. Analytical results for the base-shear-versus-top-displacement relationship corresponding to these three cases are compared with test data for Specimen B4 in Fig. C3. The
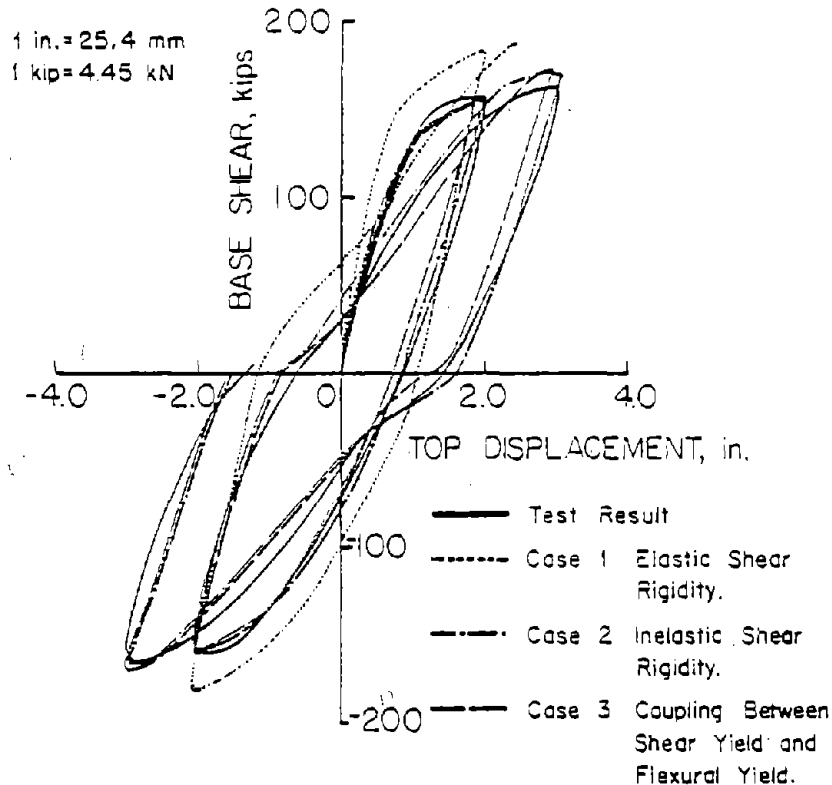
1 in.=25.4 mm
1 kip=4.45 kN

BASE SHEAR, kips
TOP DISPLACEMENT, in.

Test Result

Case 1   Elastic Shear
          Rigidity.

Case 2   Inelastic Shear
          Rigidity.

Case 3   Coupling Between
          Shear Yield and
          Flexural Yield.

Fig. C5   Base-Shear-Versus-Top-Displacement
            Relationships for Specimen B5

Measured
Case 2
Case 3
1 in = 25.4 mm
1 ft. = 0.305 m

HEIGHT, ft
DEFLECTION, in.

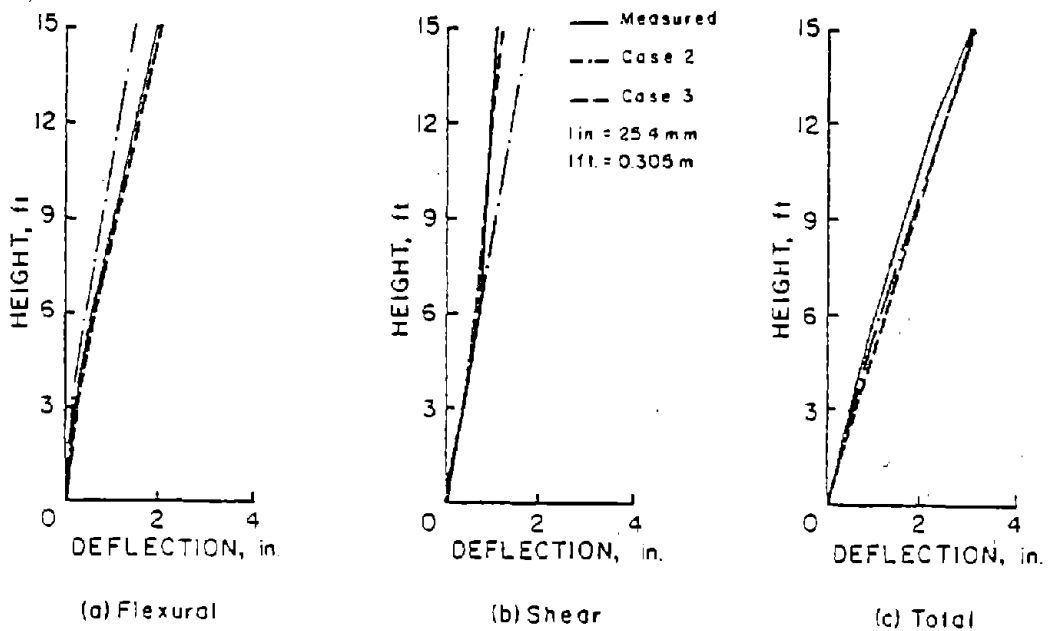(a) Flexural   (b) Shear   (c) Total

Fig. C6   Deflected Shapes for Specimen B5

analytical results for all three cases compare reasonably well with experimental data. Case 2 gives the closest agreement.

Deflected shapes corresponding to a top deflection of 9 in. are shown in Fig. C4. Figures C4 (a) and (b) show the flexural and shear components of deflection separately for Cases 2 and 3, together with the respective "measured" values. The "measured" flexural and shear components were calculated by integrating rotations and distortions recorded during the tests over a height of 6 ft and assuming a linear variation of deflection from this point to the top of the wall. Figure C4 (c) shows the total deflected shapes for these two cases together with the corresponding measured deflection.

These figures clearly show the effect of coupling between shear and flexural yielding on the deflected shape. As shown in Fig. C4 (b), if coupling is not considered, the deflected shape due to the shear component is a straight line. This follows from the fact that the shear force is constant along the height of the wall. When coupling is considered, a shape change in the slope of the wall occurs near the hinging region. This is also apparent in the experimental curve.

Specimen B5. Figure C5 shows a comparison of base shear versus top displacement relationships for the different analytical cases and the measured curve for Specimen B5. The case where a linearly elastic shear versus shear distortion relationship is assumed, slightly overestimates the absorbed energy relative to the test results. The other two cases, where inelastic shear behavior is assumed, satisfactorily reproduced
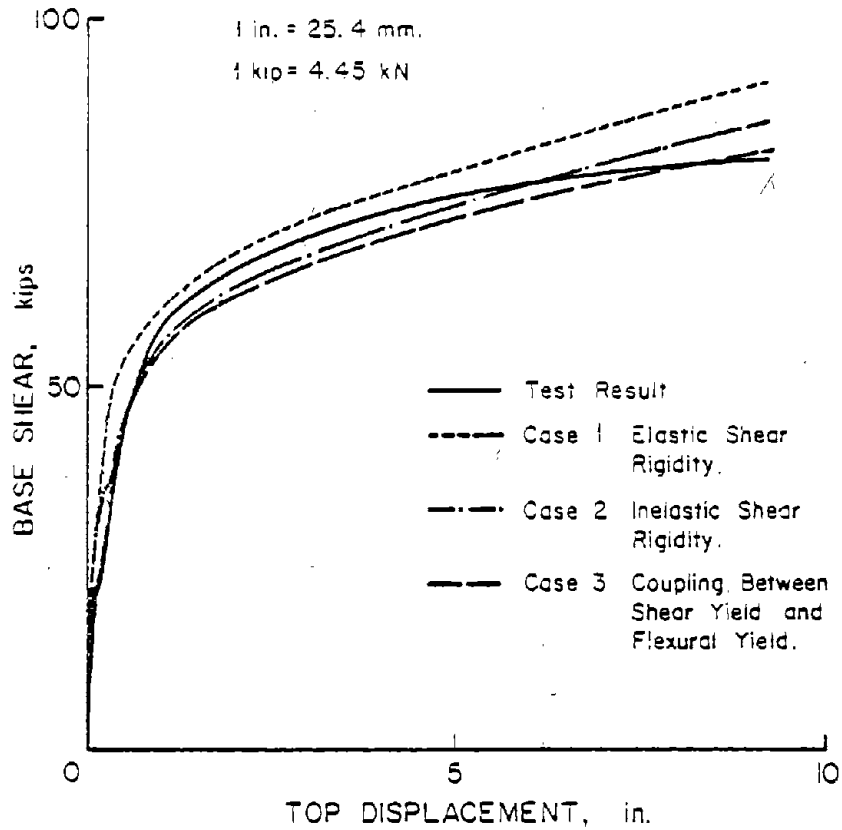
Fig. C5   Base-Shear-Versus-Top-Displacement Relations
          for Specimen B4

(a) Flexural   (b) Shear   (c) Total
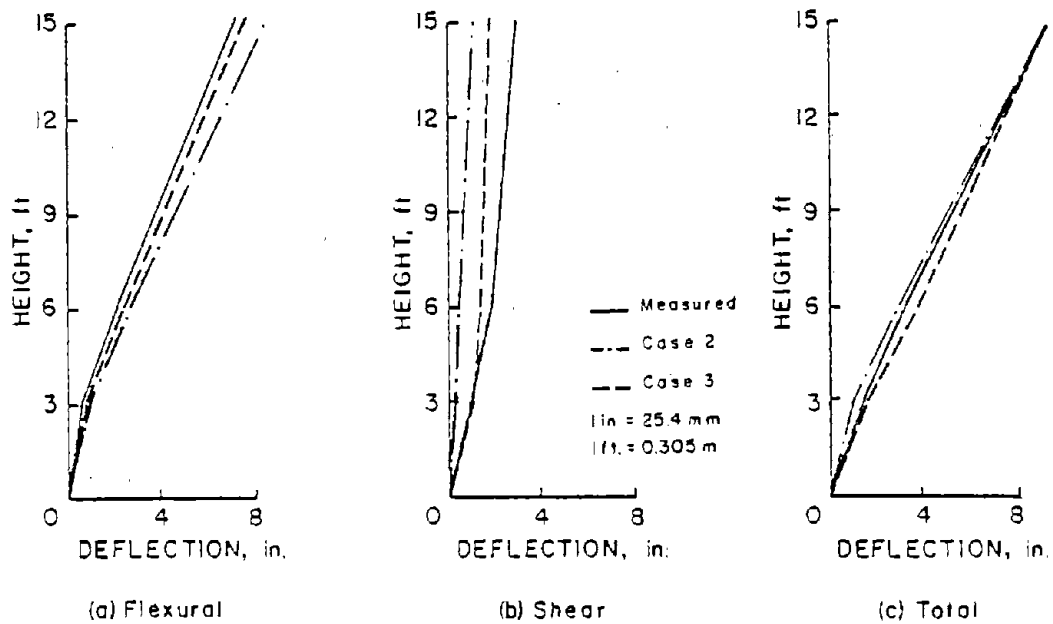
Fig. C6   Deflected Shapes for Specimen B4

the hysteresis loops recorded during the test.

Deflected shapes corresponding to the positive peak in the second cycle are shown in Fig. C6. The flexural and shear components of the deflected shape are presented separately in the figure, in addition to total deflected shapes.

Both Cases 2 and 3 satisfactorily predicted the measured total deflected shape as can be seen in Fig. C6 (c). However, Case 3, which considers the coupling between shear yielding and flexural yielding simulated the test result much closer than Case 2. This is most apparent from a comparison of analytical and test results in terms of flexural and shear components as shown in Fig. C6 (a) and (b).

Summary

Structural walls are generally designed with sufficient shear capacity to ensure that flexural yielding occurs before the shear capacity of the member is reached.

Tests conducted at the Construction Technology Laboratories indicate the almost-simultaneous occurrence of shear yielding and flexural yielding at a load level well below the calculated static shear capacity. This observation raised questions concerning the probable effects of such shear yielding in walls on the behavior of coupled wall systems.

Some validation of the analytical model was obtained by using it to reproduce observed results for selected specimens tested under slowly reversing loads. Comparisons between analytical and experimental results indicate satisfactory agree-

ment. This leads to the conclusion that the analytical model developed here can well represent the wall members of coupled wall systems.

The following observations may be made on the basis of results of this limited study. These observations strictly apply only to the cases and parameter ranges covered in the investigation.

1. Although yielding in shear concurrent with flexural yielding increases the shearing component of distortion in the hinging region of walls, its effect on the over-all behavior of walls is relatively small.

2. Use of analytical models that account for inelastic shear distortion in walls is necessary to successfully simulate the overall hysteretic behavior of isolated structural walls subjected to slowly reversed loading.

3. By including the effect of coupling between shear yielding and flexural yielding, increased distortions in the hinging region obeserved in the test were successfully simulated in the analysis.